

1-1-2004

# Characterization of noise in the lightning current derivative signals measured at the CN tower

Petros Liatos  
*Ryerson University*

Follow this and additional works at: <http://digitalcommons.ryerson.ca/dissertations>

 Part of the [Electrical and Electronics Commons](#)

---

## Recommended Citation

Liatos, Petros, "Characterization of noise in the lightning current derivative signals measured at the CN tower" (2004). *Theses and dissertations*. Paper 38.

# **CHARACTERIZATION OF NOISE IN THE LIGHTNING CURRENT DERIVATIVE SIGNALS MEASURED AT THE CN TOWER**

by

**Petros Liatos**

A thesis

presented to Ryerson University

in partial fulfillment of the

requirements for the degree of

Master of Applied Science

in the Program of

Electrical and Computer Engineering

Toronto, Ontario, Canada, 2003

© Petros Liatos 2003



National Library  
of Canada

Bibliothèque nationale  
du Canada

Acquisitions and  
Bibliographic Services

Acquisitions et  
services bibliographiques

395 Wellington Street  
Ottawa ON K1A 0N4  
Canada

395, rue Wellington  
Ottawa ON K1A 0N4  
Canada

*Your file* *Votre référence*

*ISBN: 0-612-94224-4*

*Our file* *Notre référence*

*ISBN: 0-612-94224-4*

The author has granted a non-exclusive licence allowing the National Library of Canada to reproduce, loan, distribute or sell copies of this thesis in microform, paper or electronic formats.

L'auteur a accordé une licence non exclusive permettant à la Bibliothèque nationale du Canada de reproduire, prêter, distribuer ou vendre des copies de cette thèse sous la forme de microfiche/film, de reproduction sur papier ou sur format électronique.

The author retains ownership of the copyright in this thesis. Neither the thesis nor substantial extracts from it may be printed or otherwise reproduced without the author's permission.

L'auteur conserve la propriété du droit d'auteur qui protège cette thèse. Ni la thèse ni des extraits substantiels de celle-ci ne doivent être imprimés ou autrement reproduits sans son autorisation.

---

In compliance with the Canadian Privacy Act some supporting forms may have been removed from this dissertation.

Conformément à la loi canadienne sur la protection de la vie privée, quelques formulaires secondaires ont été enlevés de ce manuscrit.

While these forms may be included in the document page count, their removal does not represent any loss of content from the dissertation.

Bien que ces formulaires aient inclus dans la pagination, il n'y aura aucun contenu manquant.

**Canada**



## **Abstract**

### **CHARACTERIZATION OF NOISE IN THE LIGHTNING CURRENT DERIVATIVE SIGNALS MEASURED AT THE CN TOWER**

**© Petros Liatos 2003  
Master of Applied Science  
Department of Electrical and Computer Engineering  
Ryerson University**

Simultaneous measurements of parameters of CN Tower lightning strikes have been performed since 1991. The current derivative signals measured, are corrupted by a 100 kHz oscillating interference. This noise has caused substantial limitations on the usage of the CN Tower lightning current data. As a result, we became motivated to characterize it and search for its source. Furthermore identifying the low-frequency noise is expected to help in its removal and avoid it altogether in future installations.

This thesis proves that the low-frequency noise corrupting the lightning current derivative signals is the Loran-C radionavigation signal. This finding is a major contribution not only for the CN Tower lightning project but also for any other research related to measurement of lightning at tall structures. Researchers and experimentalists should be aware of the existence of the Loran-C signal and take the necessary precautions to avoid its interference effect.

## **Acknowledgments**

I would like to express my deep gratitude to my thesis supervisor, Dr. Ali M. Hussein for his continuous support, excellent guidance, insight, encouragement and financial support during the course of this work.

The financial support obtained from the Department of Electrical and Computer Engineering and the School of Graduate Studies of Ryerson University, which made my research possible, is acknowledged.

I am particularly grateful to Dr. M. Zeytinoglou for his invaluable feedback during the course of this work. Furthermore, the valuable discussions with Dr. S. Krishnan at the beginning of this work are much appreciated.

Special thanks go to Professor Emeritus W. Janischewskyj, Electrical and Computer Engineering Department, University of Toronto, Steven Sir of AZCAR, Dr. A. El-Rabbany of the Department of Civil Engineering, Ryerson University and J. Koch of the Electrical and Computer Engineering Department, Ryerson University for their practical help.

Finally, I would like to thank my fellow graduate students, M. Milewski, M.J. Islam, and K. Bitner for their help and encouragement.

# Contents

<b>List of Figures</b> .....	viii
------------------------------	------

<b>List of Tables</b> .....	x
-----------------------------	---

## 1. Introduction

1.1 The Lightning Phenomenon.....	1
1.2 CN Tower Lightning Observations.....	1
1.3 Current Measurement System.....	4
1.4 Typical Current Derivative and Current Waveforms.....	7
1.5 Types of Noise.....	12
1.6 Removal of the Low Frequency Noise.....	15

## 2. Characterization of the Low-Frequency Noise

2.1 Importance of Identifying the Low-Frequency Noise.....	19
2.2 Extraction of the Low-Frequency Component from Noise Files.....	20
2.3 Typical Noise Files.....	22
2.4 Existence of the Low-frequency Noise along the Tower's Structure.....	30
2.5 Searching for the Source of the Low-Frequency Noise.....	37

## 3. Loran-C

3.1 Introduction.....	38
3.2 Groundwave.....	44
3.3 Skywave.....	45
3.4 Groundwave versus Skywave.....	48
3.5 The Electric Field of Loran-C.....	56

## **4. The CN Tower: A Receiver of Loran-C**

4.1 Lightning as Noise for Loran-C.....	58
4.2 Is the CN Tower an efficient receiving antenna for Loran-C?.....	59
4.3 Motivation for Composing the Loran-C Signal at the Location of the CN Tower.....	60
4.4 Loran-C Stations “Close” to the CN Tower.....	61
4.5 Composition of Loran-C at the Location of the CN Tower.....	66

## **5. Conclusions and recommendations.....77**

## **References.....79**

## List of Figures

- Figure 1.1: The CN Tower and locations of instruments.
- Figure 1.2: Current derivative measurement system.
- Figure 1.3: Typical lightning current derivative captured by the old coil.
- Figure 1.4: Typical lightning current.
- Figure 1.5: Typical lightning current derivative captured by the new coil.
- Figure 1.6: Typical lightning current for new coil.
- Figure 1.7: Lightning current derivative and current captured by the old coil.
- Figure 1.8: Current derivative and current captured by the new coil.
- Figure 1.9: Current waveform after the removal of the DC offset.
- Figure 1.10: Current derivative and current, May 1st 1996.
- Figure 1.11: Current waveform passed through a 90-110 kHz bandstop filter.
- 
- Figure 2.1: Magnitude and Phase response of an integrator as a filter.
- Figure 2.2: Typical Old Coil noise file.
- Figure 2.3: Typical New Coil noise file.
- Figure 2.4: Typical old coil noise file recorded by the LeCroy digitizer, its integration and the filtered signal.
- Figure 2.5: Magnitude response of the filter.
- Figure 2.6: Typical old coil noise file, its integration and its filtering.
- Figure 2.7: FFT of a typical filtered noise waveform captured by the old coil.
- Figure 2.8: Typical new coil noise file, its integration and its filtering.
- Figure 2.9: FFT of a typical filtered noise waveform captured by the new coil.
- Figure 2.10: CN Tower coil visit.
- Figure 2.11: Optical transmitter and attenuator at the new coil location.
- Figure 2.12: New coil noise file captured before the removal of the attenuator.
- Figure 2.13: FFT of a filtered noise waveform captured by the new coil, after the removal of the attenuator.
- Figure 2.14: Test signal without the attenuator.
- Figure 2.15: Test signal with the attenuator connected.

Figure 3.1: Loran-C pulse groups and sequencing.

Figure 3.2: Loran C pulse and its frequency spectrum.

Figure 3.3: Loran-C transmitting antenna.

Figure 3.4: Groundwave and Skywave paths.

Figure 3.5: Skywave delay vs range.

Figure 3.6: Electric field strength for groundwave calculated analytically.

Figure 3.7: Electric field strength for skywave calculated analytically (nighttime).

Figure 3.8: Groundwave field strength for 100 kHz (ITU Recommendation P.368-7).

Figure 3.9: Skywave field strength for summer night.

Figure 3.10: Analytical vs published field strengths.

Figure 3.11: Published field strengths for groundwave and skywave.

Figure 3.12: Electric field for a master station pulse group and its spectrum.

Figure 4.1: Loran-C transmitting antenna in Malone, with background lightning.

Figure 4.2: Loran-C Stations “close” to Toronto.

Figure 4.3: Electric field of 9960 chain at the location of the CN Tower for daytime.

Figure 4.4: Electric field strength of one Seneca station pulse for daytime.

Figure 4.5: Electric field strength of one Seneca station pulse for nighttime.

Figure 4.6: Electric field strength of one Caribu station pulse for daytime.

Figure 4.7: Electric field strength of one Caribu station pulse for nighttime.

Figure 4.8: Electric field calculated at the location of the CN Tower due to each of the stations of table 4.2 for nighttime.

Figure 4.9: Composite signal of the electric field of Loran-C at the CN Tower for nighttime.

Figure 4.10: Spectrum of simulated Loran-C signal at the CN Tower.

Figure 4.11: Loran-C signal recorded in Denmark.

Figure 4.12: Noise signal recorded at the CN Tower.

## **List of Tables**

Table 3.1: Polynomial coefficients.

Table 4.1: Loran-C stations close to Toronto and their functions.

Table 4.2: Comprehensive table of stations close to Toronto.

# Chapter 1

## Introduction

### 1.1 The Lightning Phenomenon

Lightning is one of the most fascinating events of nature. Although the preliminary understanding of the lightning phenomenon was established by Benjamin Franklin early in the eighteenth century, it is still one of the major subjects in modern research [1]. The present research interest in the lightning area is mostly concerning the protection of electrical and electronic components that are exposed to hazards of lightning such as those used in electric power lines, telecommunication systems, aircrafts and spacecrafts. Since more sensitive electronic devices are used nowadays, protection from lightning hazards has become more important than ever. In the meantime the development of high speed, high quality measurement methods makes it possible to study the characteristics of lightning more precisely and efficiently.

### 1.2 CN Tower Lightning Observations

Statistical information on characteristics of lightning is of primary interest for such areas of study as insulation coordination of power lines and substations and protection of tall structures and neighboring buildings. Over the two last decades, the North American Lightning Detection Network (LDN) has been utilized for lightning protection of North American forests and electric power lines. As part of its regular data collection, the LDN is capable of accumulating a vast amount of lightning information. Attempts to use this

database for determination of local lightning severity have indicated that the radiation models used do not adequately reflect the propagation of electromagnetic waves caused by lightning. In particular, because a simplified radiation model is used by the Lightning Location and Protection Inc. (LLP) systems, derivation of the lightning current peak from the recorded peaks of the lightning-generated electromagnetic pulses (LEMP) may be associated with considerable error. In fact, simultaneous measurement of the lightning current and the corresponding electric and magnetic fields, and of lightning channel characteristics is necessary not only for the calibration of the LDN systems, but also for the quantitative assessment of presently used lightning radiation models. Such assessment would permit better utilization of the huge amount of data collected yearly by the LDN systems, already installed in North America including the “young” Canadian Lightning Detect Network (CLDN), which started operating in 1997. Furthermore, positively assessed radiation models are needed as the basis for calculating power line overvoltages caused by lightning.

It is observed that tall structures receive many more lightning strikes than plain ground. Traditionally, they are very useful in studying characteristics of lightning. The Toronto Canadian National (CN) Tower, with a height of 553 m, is the tallest manmade, freestanding structure in the world. While the local lightning flash density in Toronto is less than two flashes per square kilometer per year, the CN Tower usually receives many tens of direct strikes each year [2,3]. During the 1991 lightning season, for instance, the tower was hit with 72 flashes, 24 of which occurred within 100 minutes in the early morning of July 7. It is important to note that the most valuable lightning parameter is the

lightning current. This is because of the general difficulty of measuring the lightning current, which necessitates the use of a very tall structure, a moderately tall structure erected on high ground, or the utilization of rocket- or laser-triggered lightning. Therefore, the CN Tower presents one of the best sites in the world to observe lightning for the purpose of studying the physics of tall structure lightning, assessing and developing lightning return-stroke models at elevated objects [4,5], and collecting characteristics of visual parameters [3], of currents [6,7] and of lightning-generated electromagnetic fields [8].

Lightning strikes to the CN Tower have been monitored since 1978, two years after its erection. Successful simultaneous measurements of significant parameters of CN Tower lightning strikes have been performed since the summer of 1991 [2]. By the summer of 1991, five measurement stations were operating to simultaneously measure seven of the most important lightning parameters. The measurements obtained include the current derivative recorded at the CN Tower, the corresponding electric and magnetic fields detected 2 km north of the tower, and the lightning channel characteristics. The lightning channel characteristics are obtained using two VHS cameras (for the construction of three dimensional images), a High Speed Camera (HSC) and a Return Stroke Velocity (RSV) photodiode measuring system. Figure 1.1 shows the locations of the instruments.

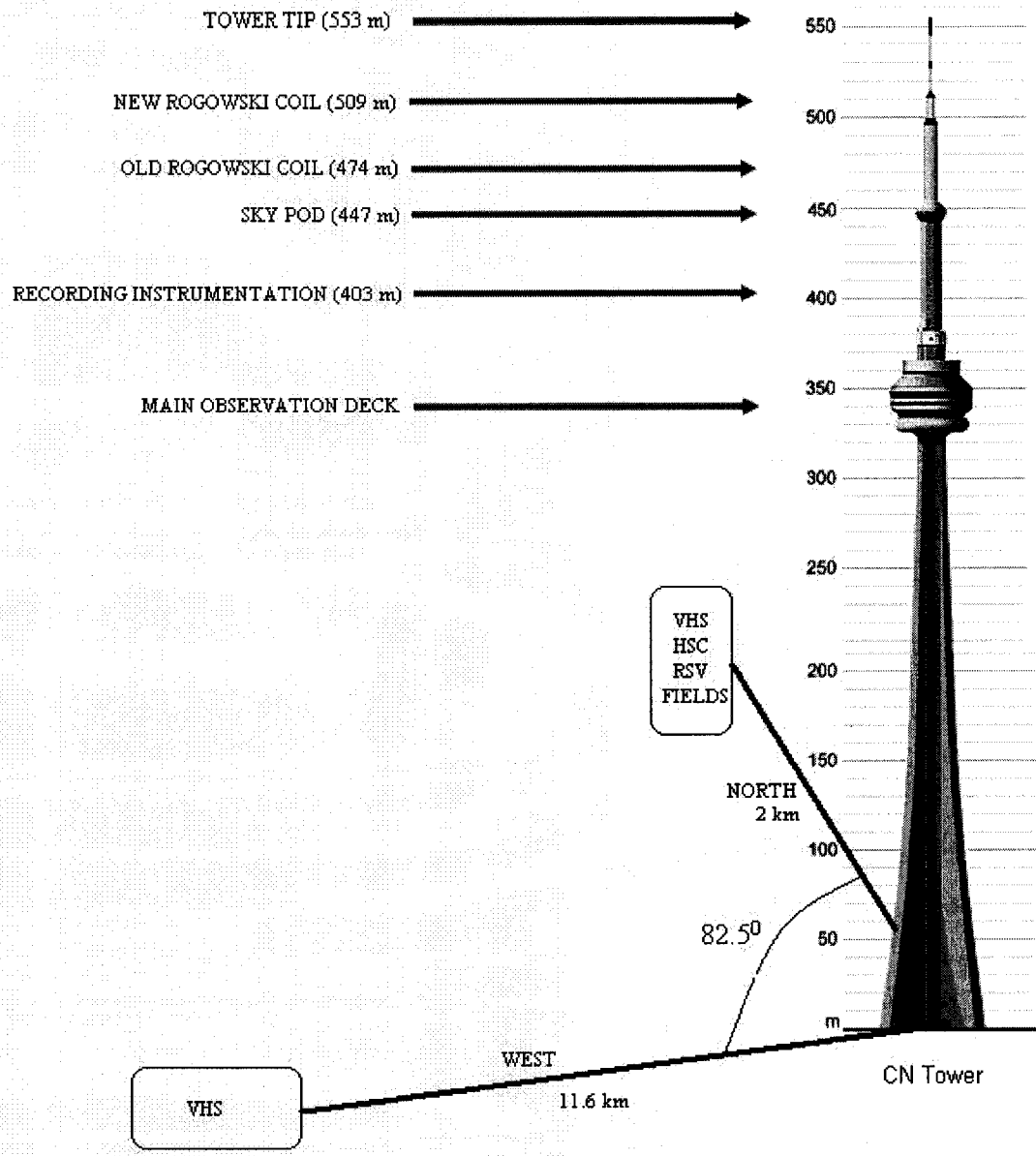


**Figure 1.1: The CN Tower and locations of instruments.**

### 1.3 Current Measurement System

Let us take a closer look at the current derivative measurement system installed at the CN Tower. The system, installed in 1990, utilizes a 3m, 40 MHz Rogowski current sensing

coil. The coil encircles one fifth of the tower's steel structure at the 474m above ground level (AGL). Above the Sky Pod (447 m AGL), the tower's steel structure has five identical plates joined together to form a cylinder with a pentagon cross-section. At the 474m AGL, each steel plate has an elliptically shaped hole at its center. The Rogowski coil encircles one of the five corners going through the adjacent elliptically shaped holes. Because of the symmetry, the captured signal is assumed to correspond to 20% of the total current. The coil is connected, via a tri-axial (double shielded) cable, to a recording station placed at the 403m AGL. The current derivative recording station consists of a 10 ns, 10 bit, double channel computer-controlled digitizer with segmented memory (Tektronix RTD710A). The maximum sampling rate for the digitizer is 100 MHz for both channels. Prior to the summer of 1997 both channels of the digitizer measured the lightning current derivative signal with the channels set at different scales in order to enhance vertical resolution. This current derivative station is set to capture up to eight return strokes. (Each lightning flash may consist of one or more lightning return strokes.)

During the summer of 1997, a noise-protected current derivative measurement system was installed at the tower. This system features a 6m, 20 MHz Rogowski coil surrounding the entire steel structure of the tower at the 509m AGL and is connected to the recording station via an optical fiber link. The current derivative records captured by this new Rogowski coil have a superior signal-to noise ratio than those recorded by the old system because the new system captures the whole current derivative signal and utilizes an optical fiber link. As shown in Figure 1.1, the two current sensors were installed as far as possible from the tower's main structural discontinuities (the tip of the

tower, the Sky Pod, the top and bottom of the Main Observation Deck, and the ground level) in order to capture the current waveform free from reflections, at least for fast rise waveforms. In 2003 a new digitizer (LeCroy Waverunner) was installed at the CN Tower in order to record more efficiently the current derivative signals. However, both digitizers are still in use at the CN Tower. The LeCroy digitizer is an 8-bit, 2ns, double channel digitizer with segmented memory and its maximum sampling rate is 500 MHz. The memory of the LeCroy digitizer is 1 M points per channel in dual channel mode, much more superior to the 128 K points per channel for the Tektronix digitizer [9]. For most of the work done in this thesis the LeCroy digitizer was used. Figure 1.2 shows a block diagram of the current derivative measuring system.

The current derivative system is real time operating 24 hours a day, 365 days a year. When lightning strikes the CN Tower, the output voltage of the coils, exceeds a threshold set at the digitizers, and the digitizers are triggered. This way the lightning current derivative waveform is stored together with a predetermined pre-return-stroke time window.

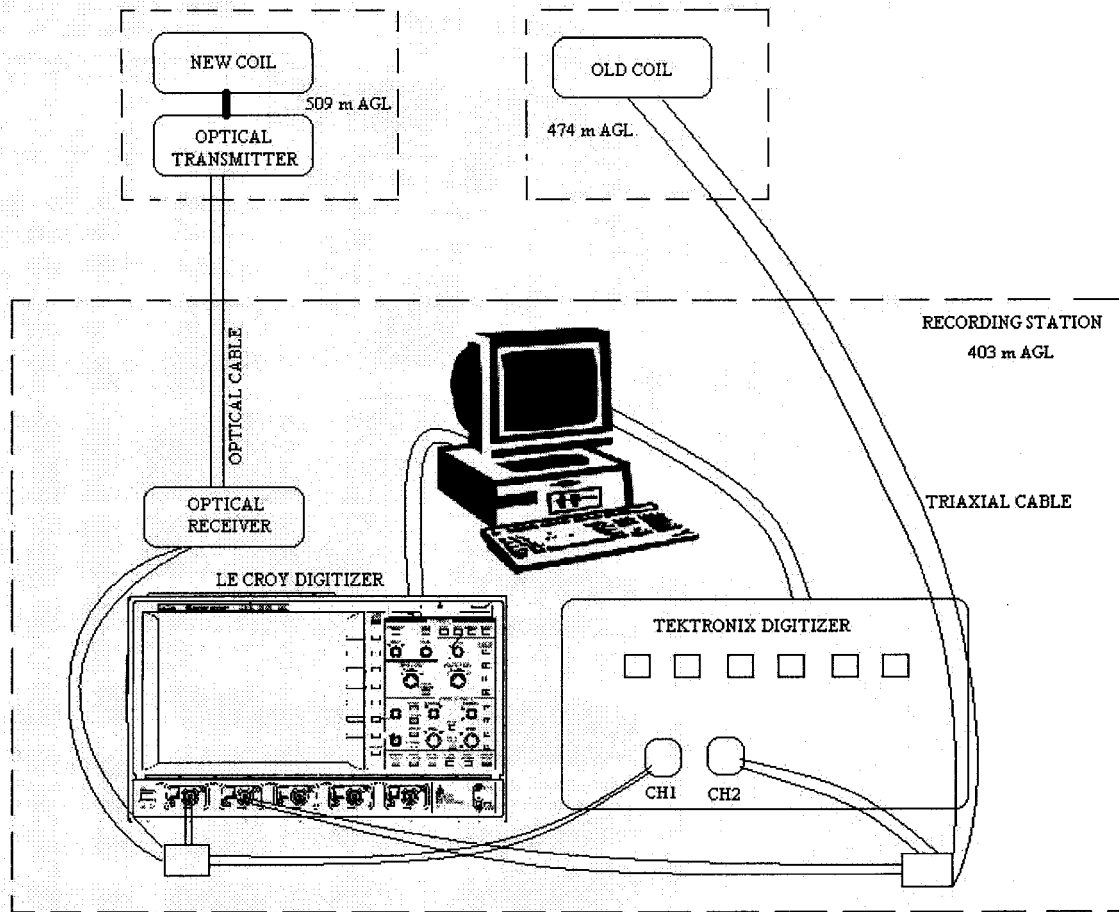
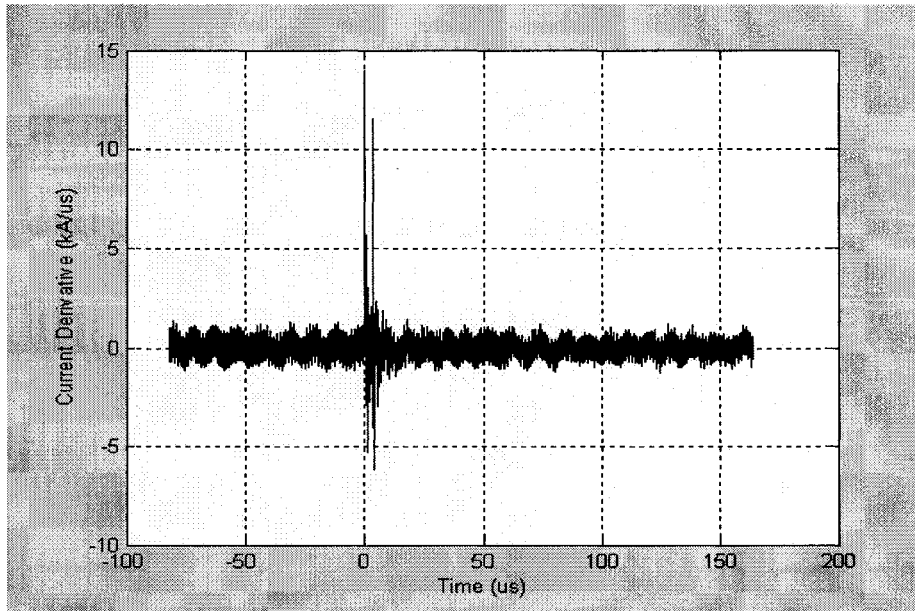


**Figure 1.2: Current derivative measurement system.**

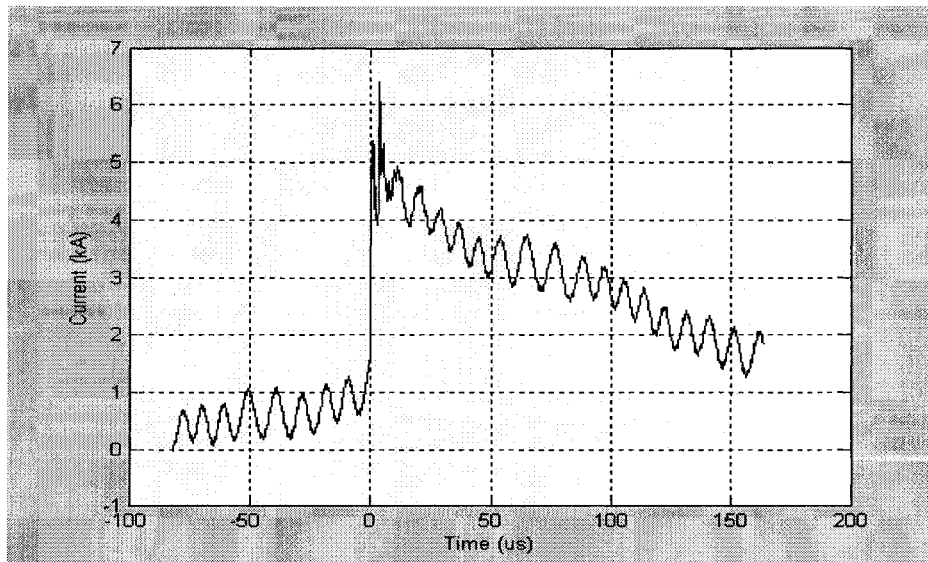
### 1.4 Typical Current Derivative and Current Waveforms

Figure 1.3 shows a typical waveform of a current derivative ( $di/dt$ ) signal captured by the old coil. Each  $di/dt$  record contains 16 kilobytes of data recorded at 100 MHz or 10 ns time resolution. This current derivative waveform was captured on June 20, 1997 at 13:54:51 and is the seventh lightning stroke of an eight-stroke flash. In this waveform, the last 2 kb of data has been sampled at 20 MHz, in order to obtain a larger time window at the decay part of the current waveform.

Figure 1.4 shows a typical current waveform obtained from the signal shown in Figure 1.3 by numerical integration



**Figure 1.3: Typical lightning current derivative captured by the old coil.**



**Figure 1.4: Typical lightning current.**

A typical current derivative waveform and its corresponding current, are shown in Figures 1.5 and 1.6 respectively. This stroke is the fourth stroke of a four-stroke flash captured on April 11, 1999 at 12:55:34.

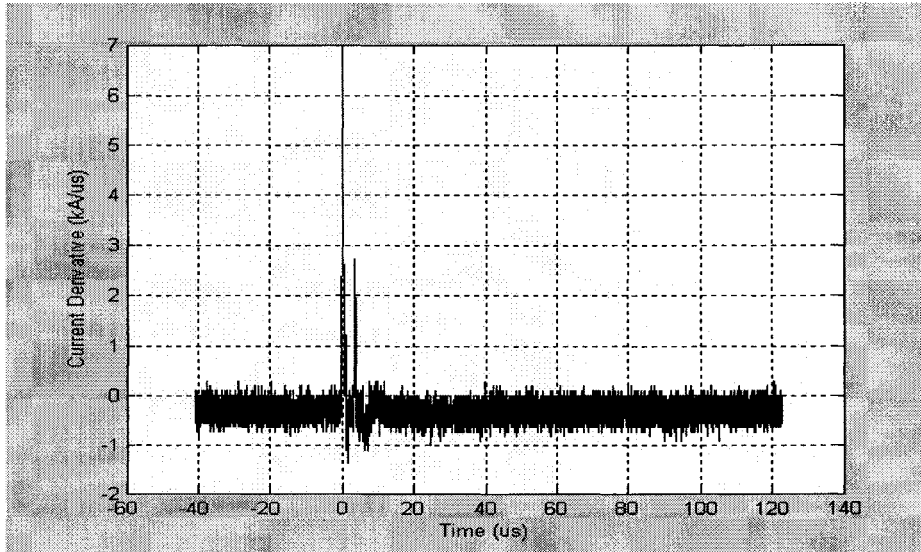


**Figure 1.5: Typical lightning current derivative captured by the new coil.**

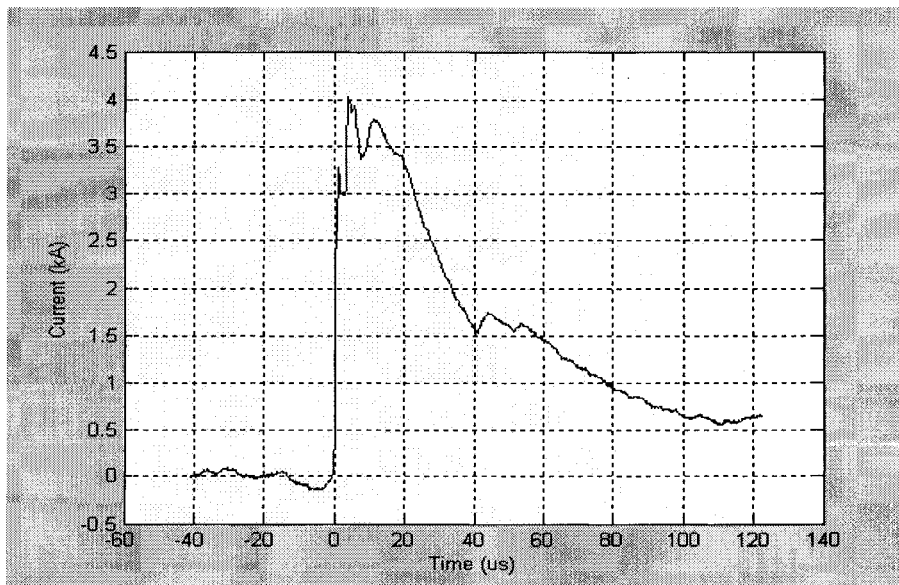


**Figure 1.6: Typical lightning current for new coil.**

To make a better comparison between signals captured by the old coil and the new coil current measurement systems, we need to see a lightning stroke waveform captured by both systems simultaneously. Figures 1.7 and 1.8 show the current derivative and current of the exact same stroke, from the old and new coils respectively. This lightning stroke occurred on January 2, 1999 at 22:27:04. The figures demonstrate the substantially better signal-to-noise ratio of the new coil system.

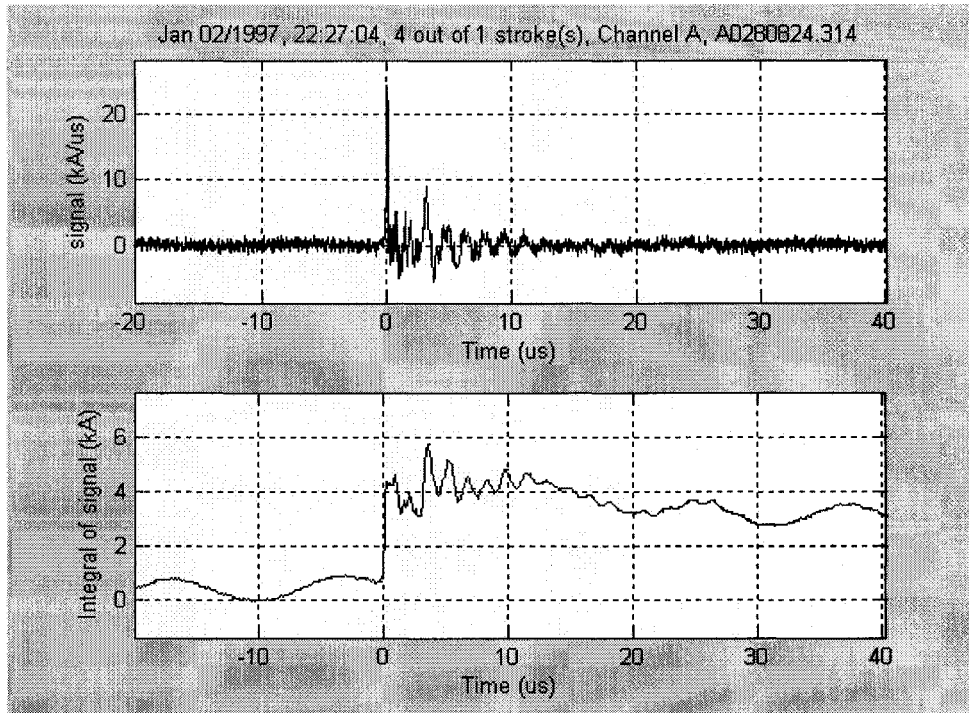


**Figure 1.7: Lightning current derivative and current captured by the old coil.**

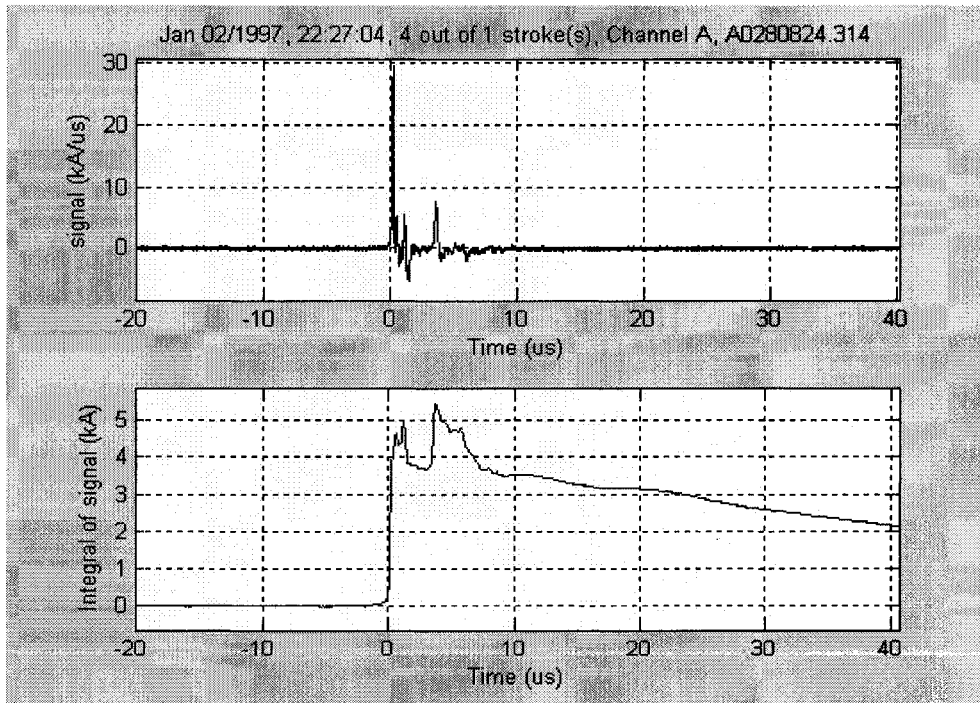


**Figure 1.8: Current derivative and current captured by the new coil.**

## 1.5 Types of Noise

The CN Tower is a transmission tower and it is expected that the lightning current signals be corrupted by noise. By looking at Figures 1.3-1.6 we can identify the various types of noise.

### A. DC Offset

From Figure 1.4 it can be seen that there is a ramp in the current waveform. That ramp is the result of a DC offset in the current derivative. It is easy to remove this noise by averaging the pre-lightning portion of the signal and then subtracting it from the whole signal. In fact we can also remove the very small DC offset from the current as well. After these operations at the signal of Figure 1.3 we obtain a signal with no DC offset as seen in Figure 1.9.

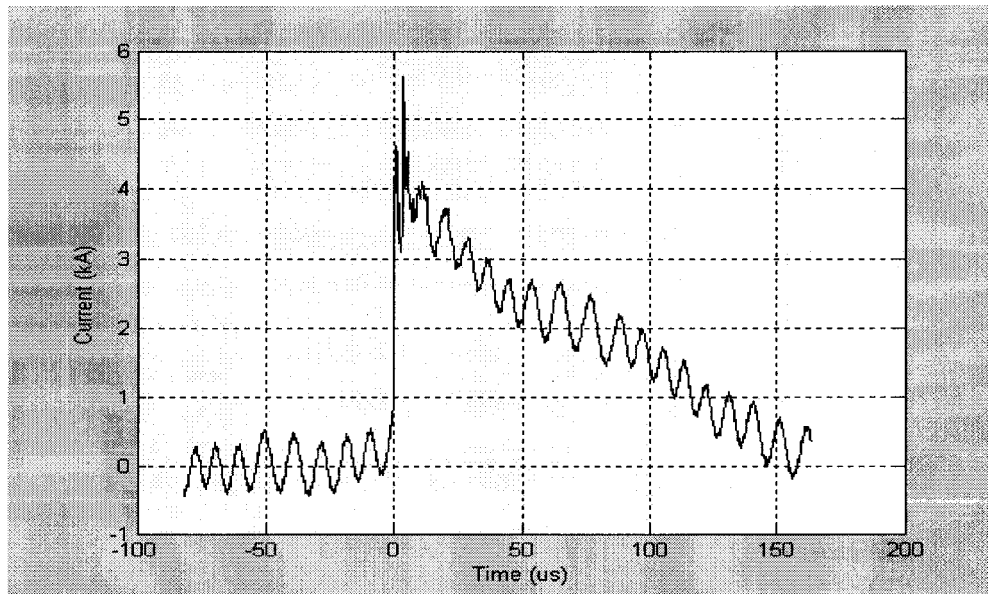


**Figure 1.9: Current waveform after the removal of the DC offset.**

### B. High Frequency Noise

This type of noise does not affect much the waveforms. Usually the  $di/dt$  peak is much higher than the high frequency noise and so it does not cause problems. Furthermore integration works as a low pass filter and thus the current waveform (obtained through integration) does not suffer from the high frequency noise. In a few words, the effect of high frequency noise is minimal.

### C. Low Frequency Noise around 100 kHz

This noise has an order of magnitude usually comparable to the lightning signal. It can be seen very clearly in Figure 1.4 how much it affects the signal. Usually we are interested in calculating the current waveform parameters. However, the existence of the low-frequency noise, makes the calculation of the waveform parameters difficult since we cannot confidently identify the base level, peak, maximum steepness and 10-90% risetime. Furthermore, it makes the calculation of some waveform parameters, such as half-peak pulse width, almost impossible. For this reason, only limited statistics concerning current wavefront parameters (maximum wavefront steepness, peak and 10-90% risetime) have been established [9]. The extraction of wavefront parameters has been done manually due to the presence of the noise. When a waveform has slow rise and low current peak the effect of the noise is even more severe. There is a substantial number of captured waveforms which are completely unusable because of the existence of noise. Figure 1.10 shows one example of a current derivative waveform captured on May 1<sup>st</sup>, 1996. In this case, the lightning signal is completely embedded in the low-frequency noise and it is almost impossible to calculate any parameters.

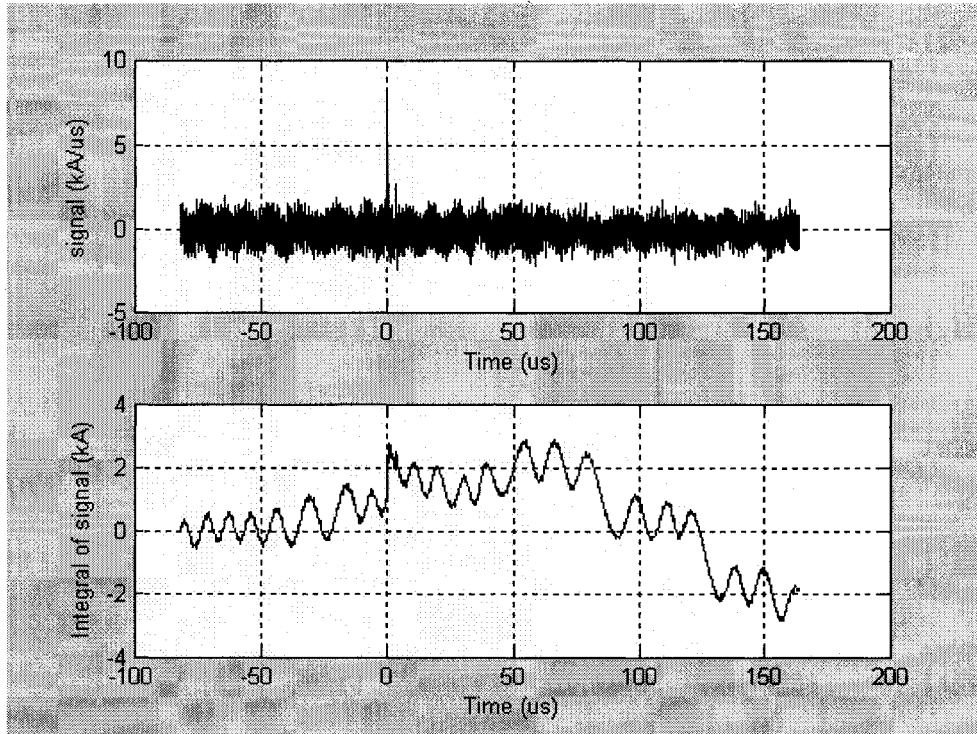


**Figure 1.10: Current derivative and current, May 1st 1996.**

This type of noise is also the most problematic to remove. It is not visible in Figure 1.6 since the new coil system effectively shields the waveform from this type of noise. However, it is very important to effectively remove it from current derivative signals recorded via the old coil for a number of reasons. First, there is a huge amount of data captured by the old coil from 1991 until now (13 years). In order to use this amount of data effectively we need to remove the noise. Furthermore, the new coil has not been working properly for most of the time since installed so we very much still rely on the old coil for statistical analysis of current waveform parameters. Finally, the old coil has a bandwidth of 40 MHz whereas the new coil has a bandwidth of 20 MHz.

#### D. Reflections

Current reflections do not classify literally as noise, but depending on the current wavefront steepness they may alter the shape of the lightning waveform and hence complicate the calculation of waveform parameters (peak, maximum steepness, risetime and pulse width at half peak). They are caused by structural discontinuities of the tower when the lightning propagates through the tower. The reflections can be seen very clearly in Figure 1.6. After the first peak there are several distinct peaks corresponding to different discontinuities in the tower [10]. In case of signals captured by the old coil, the main reflection occurs always 3.16  $\mu\text{s}$  after the first peak and it is associated with the ground. Lightning propagates through the tower almost with the speed of light. The distance between the old coil and the ground is 474 m so lightning current needs 3.16  $\mu\text{s}$  to travel from the old coil to the ground and back. Other reflections have smaller effect on the waveform. This is why we consider the first peak as the actual peak of the lightning current signal even if the second peak has larger amplitude. However, sometimes the current has a very large risetime and ground reflection reaches the old coil before the actual current peak has been reached [11].

### **1.6 Removal of the Low Frequency Noise**

Over almost the past decade, there has been a lot of work in trying to remove the low-frequency noise. The most obvious way of removing the noise would be to use a band stop filter and suppress the frequency band that the noise occupies. The frequency band of the noise had been calculated to occupy a frequency band of approximately 90-110

kHz. However, lightning contains information in this frequency band. By using such a filter we would distort the underlying lightning signal. Furthermore, the design of such a filter is quite difficult. The sampling rate used to capture lightning is 100 MHz. The reason we use such a high sampling rate is that the current derivative can be very steep. We have observed current derivative risetimes of as low as 47 ns [6] and consequently it is imperative that we use 100 MHz sampling rate. The stop-band of 90-110 kHz is very narrow compared to this sampling frequency. As a result the design of such a filter requires a very large number of coefficients. This poses a problem in the design and implementation of the filter because it would be highly susceptible to finite wordlength effects.

Figure 1.11 shows the lightning stroke of Figure 1.9 after being passed through a bandstop filter at 90-110 kHz. Comparing the result with Figure 1.9 we can clearly see the distortion of the lightning signal.

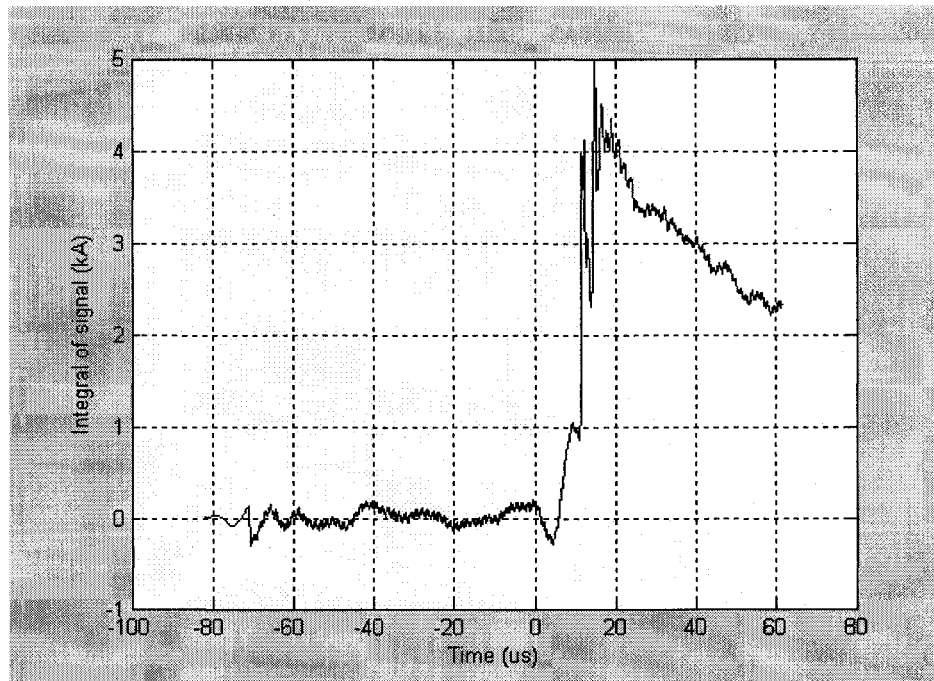


**Figure 1.11: Current waveform passed through a 90-110 kHz bandstop filter.**

In order to remove the low-frequency noise component, various alternative methods have been used until now, some of which have been quite successful. The most successful trials have been performed by M. J. Islam using Short Term Fourier Transform-Based Spectral Subtraction [12] and by O. Nedjah using Wavelet Theory [13]. In the former case Short Term Fourier Transform (STFT) was explored to analyze non-stationary signals and to deal with the limitations of Discrete Fourier Transform (DFT). A simulated current derivative waveform was artificially distorted by a noise signal measured at the CN Tower in the absence of lightning. The Spectral subtraction method proved to produce a result very close to the original simulated waveform. In the latter case Wavelet Transform by using a specific wavelet function was tried for denoising the current derivative waveforms.

In the past, other methods that were tried included linear filtering techniques by A. Obaid [14], extraction of nonstationary sinusoids by A.K Ziarani [15] and modification of the fast Fourier Transform of the lightning signal by M. Islam [16], all with moderate results.

During the work of this thesis, adaptive signal processing [17,18] and nonlinear filtering (median filtering) [19,20] were tried as means of removing the low-frequency noise. These methods however, did not produce better results from the previously mentioned ones and hence are not included in this thesis.

# Chapter 2

## Characterization of the Low-Frequency

### Noise

#### 2.1 Importance of Identifying the Low-Frequency Noise

In the past many years while the emphasis has been placed on the removal of the low-frequency noise no serious attempt has ever been made to characterize this low-frequency noise and determine its source. It has been nearly 13 years since the old coil has recorded the first noisy signals and during these years the researchers working on the CN Tower lightning project, haven't made serious effort to characterize this noise or search for its source.

There was always a question of whether this low-frequency noise was some signal received by the tower or something possibly local, related to the current measurement system. The existence of this low-frequency noise has caused substantial limitations on the usage of CN Tower lightning current data. As a result of this, we became motivated to characterize it and search for its source. Furthermore identifying the low-frequency noise might help in removing it and avoid it altogether in future installations.

## 2.2 Extraction of the Low-Frequency Component from Noise Files

In Chapter 1, we saw that when we integrate the current derivative in order to obtain the current, the high frequency component of the noise is almost eliminated. However the low-frequency component remains. We commented that this happens because the integration process works as a low-pass filter. But what exactly the kind of filtering does an integration correspond to? Let us take a closer look at integration as an act of filtering. The operation of integration is performed in Matlab using the trapezoidal rule. The output sample  $y(n)$  is obtained by the cumulative summation of all previous input samples  $x(n)$ . The first and last samples are taken with a factor of  $\frac{1}{2}$ .

$$y(n) = \frac{1}{2}x(1) + \frac{1}{2}x(n) + \sum_{k=2}^{n-1} x(k) \quad (2.1)$$

It then follows:

$$y(n) - y(n-1) = \frac{1}{2}[x(n) + x(n-1)] \quad (2.2)$$

This difference equation results in the transfer function:

$$H(z) = \frac{Y(z)}{X(z)} = \frac{1}{2} \frac{1+z^{-1}}{1-z^{-1}} \quad (2.3)$$

We can enter the filter coefficients in Matlab software to obtain the magnitude response of the integrator as a filter. Figure 2.1 shows this magnitude and phase response. The sampling frequency  $F_s$  is represented with  $2\pi$ .

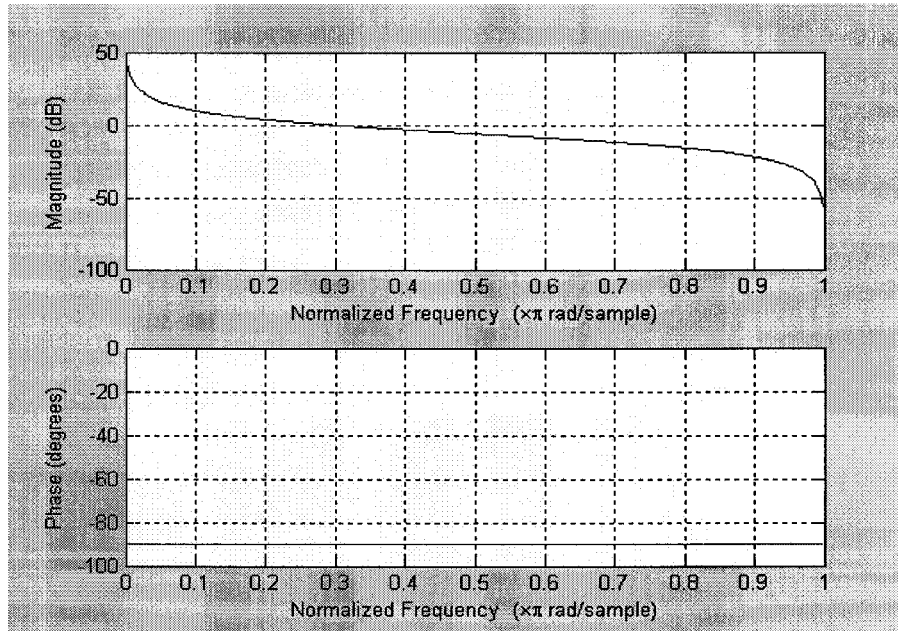


**Figure 2.1: Magnitude and Phase response of an integrator as a filter.**

It is obvious that integration works as a very smooth filter. The sampling frequency used when capturing lightning is, as mentioned before, 100 MHz. In Figure 2.1,  $\pi$  corresponds to 50 MHz. The frequency around 100 kHz corresponds to  $0.02\pi$ . From the figure we can see that in the frequency band around  $0.02\pi$  (100 kHz) the magnitude response is varying substantially. This means that the different frequencies around 100 kHz will be affected differently. So the integrated noise signal does not represent the actual measured noise component oscillating around 100 kHz.

In order to reveal the actual underlying noise signal, filtering must be used instead. However, a point of consideration should be the sampling frequency. Narrowband digital filters are characterized by sharp transitions between the passband and stopbands, and by passbands which are very small compared with the sampling frequency. As a result narrowband filters require a very large number of coefficients. This poses a problem in the design and implementation of such filters because they are highly susceptible to finite wordlength effects (for example roundoff noise and coefficient quantization errors) [21]. That is why using 100 MHz as a sampling frequency is not a recommended way for examining the low frequency noise.

In spite of having a very large number of noise files we had to capture new waveforms using a more suitable sampling rate. Most of the noise samples were captured at 1 MHz. Furthermore, the fact of using lower sampling rate allows to get much bigger time windows and examine the noise more thoroughly. However, it is also useful to examine noise files when integrated because that is what we see in the lightning records.

### **2.3 Typical Noise Files**

First we will see some noise waveforms from the old and new coils and the integration of them. Figure 2.2 shows a typical noise file from the old coil and its integration. The amplitude of the noise is about 200 mV peak to peak. After the integration the low-frequency noise is obvious as expected. Figure 2.3 shows a typical noise file from the new coil. The noise amplitude is much smaller this time being about 20 mV peak to peak.

This is of course due to the shielding effect of the optical fiber link that the new coil measurement system provides. The figure shows no trace of the low-frequency noise in the new coil noise sample. Note: The old coil and new coil noise files shown are captured at the same instant.

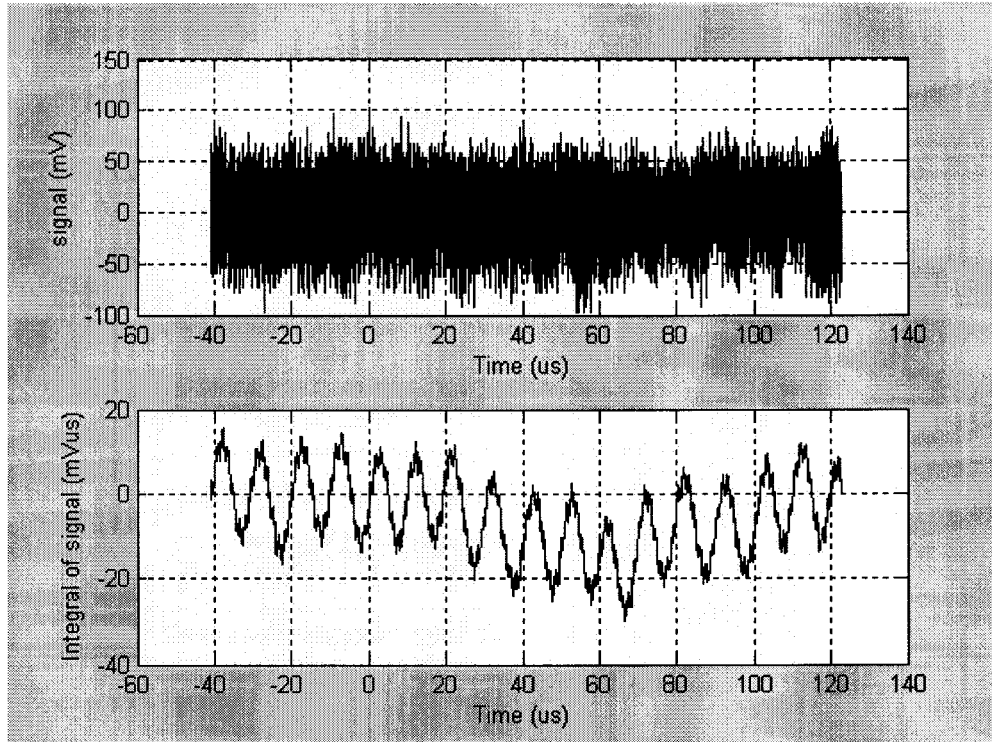


**Figure 2.2: Typical Old Coil noise file.**

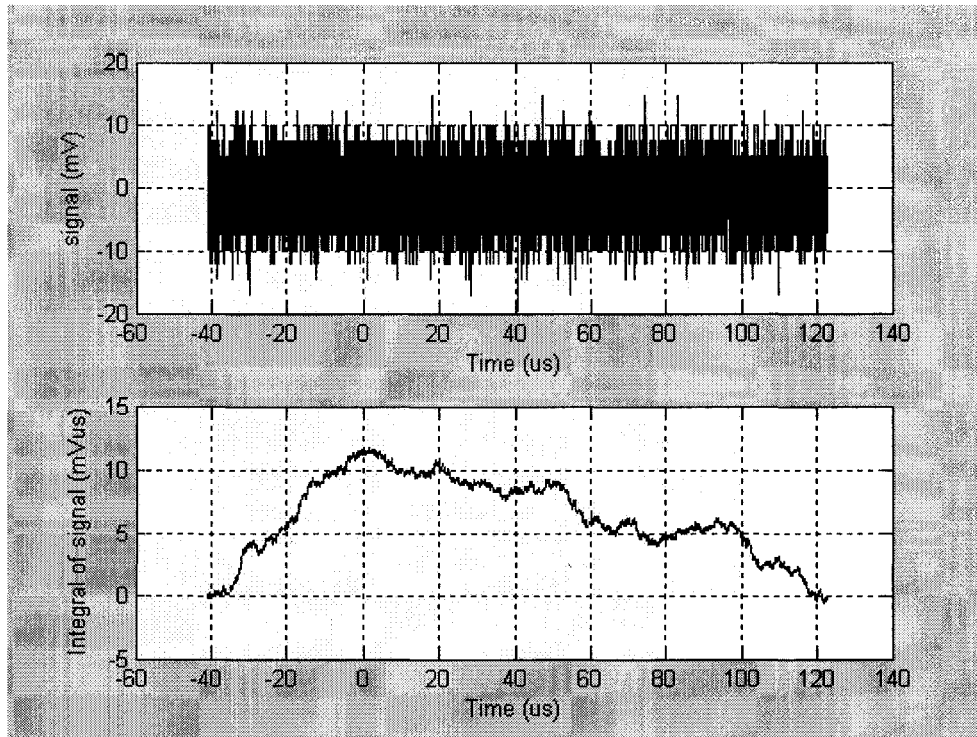


**Figure 2.3: Typical New Coil noise file.**

Figure 2.4 shows a typical noise file from the old coil recorded at 1 MHz using the new LeCroy digitizer. In the same figure we can see the integration of the noise file as well as the filtered signal using a lowpass filter with a passband edge of 200 kHz and a stopband edge of 210 kHz. The magnitude response of the filter used can be seen in Figure 2.5. The time window here is 100 ms which means that we see a large portion of the signal but we cannot see details of the signal. (the low-frequency cannot be seen because it is compressed).

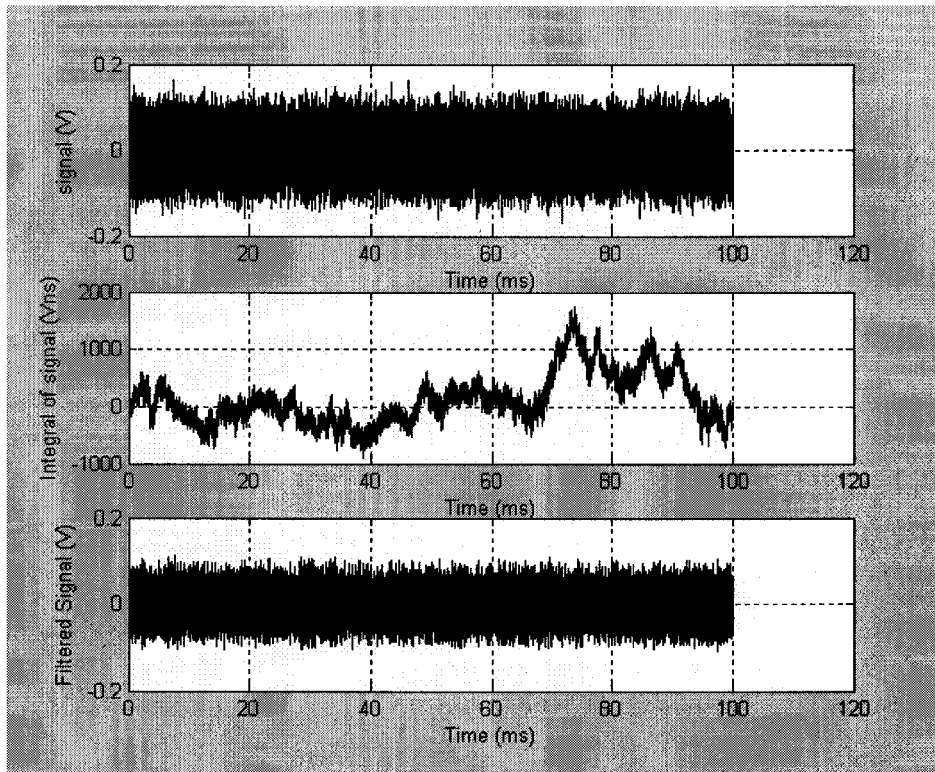


**Figure 2.4: Typical old coil noise file recorded by the LeCroy digitizer, its integration and the filtered signal.**

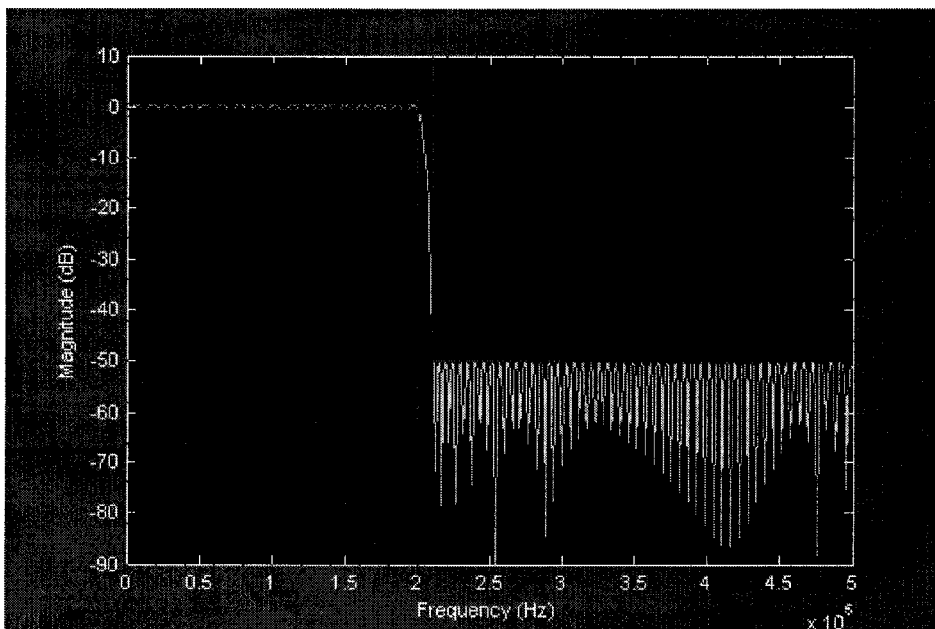


**Figure 2.5: Magnitude response of the filter.**

If we look at a much smaller portion of the signal, we will be able to clearly see again the low-frequency noise. Figure 2.6 shows only a small random portion of the signal shown in Figure 2.5 (21.5  $\mu$ s - 22  $\mu$ s). Now the low-frequency noise is visible and we can also see the difference between the integrated signal and the filtered signal.

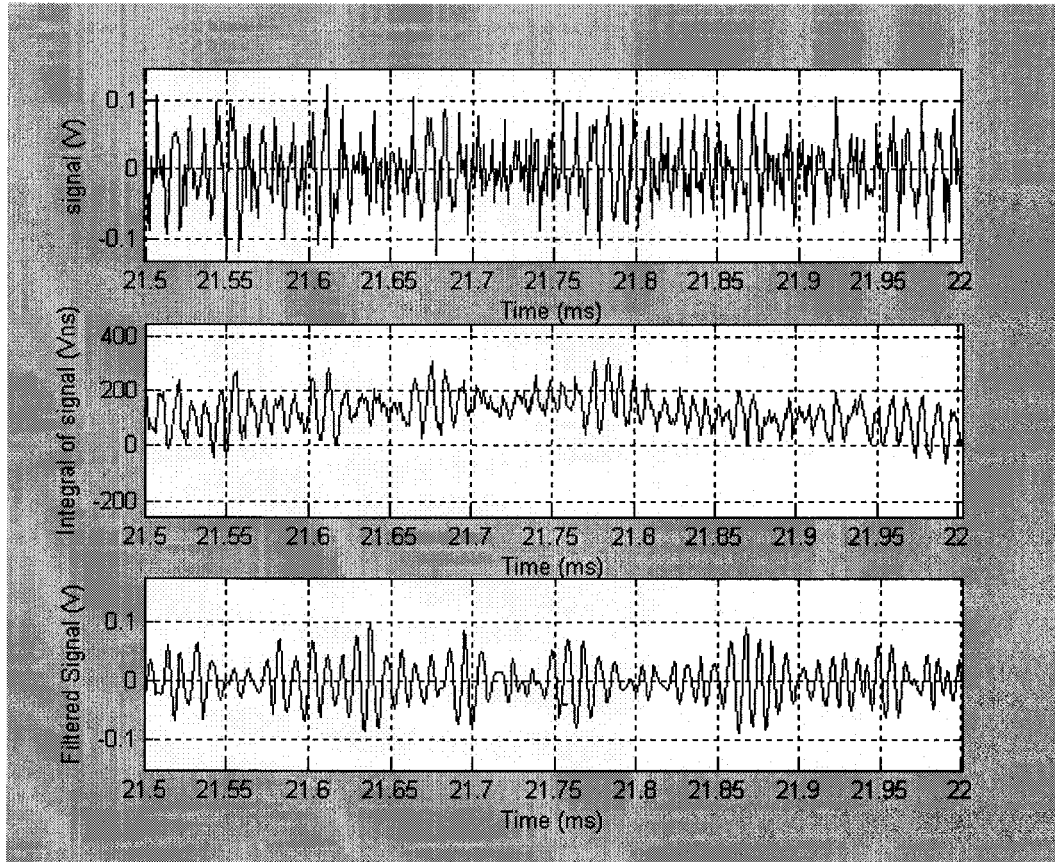


**Figure 2.6: Typical old coil noise file, its integration and its filtering.**

The spectrum of the old coil filtered noise waveform, using Fast Fourier Transform (FFT), is shown in Figure 2.7.

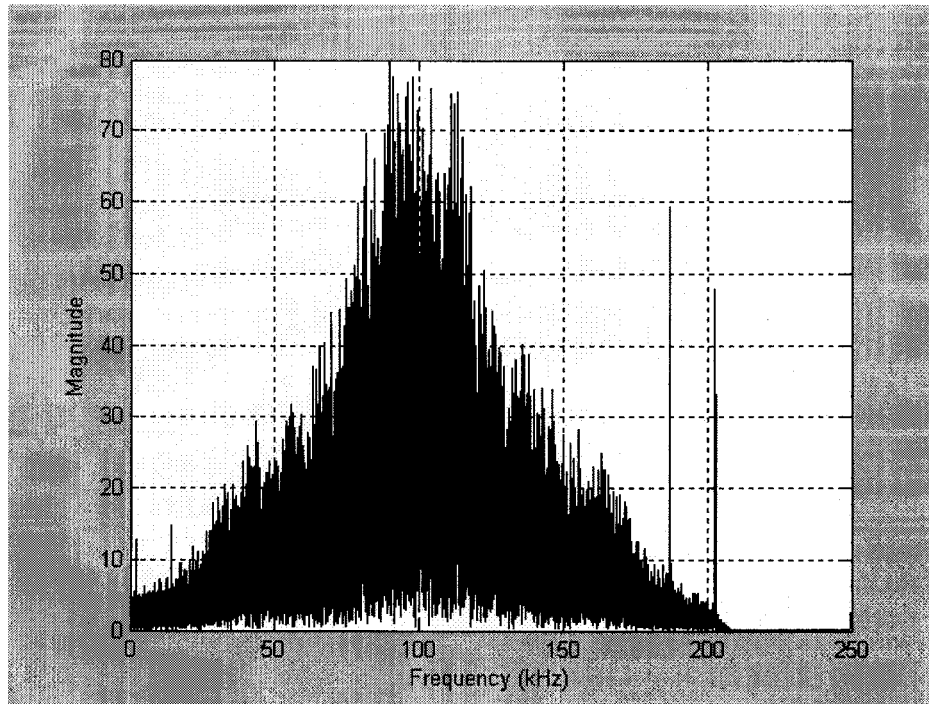


**Figure 2.7: FFT of a typical filtered noise waveform captured by the old coil.**

Now, for comparison let us see a typical new coil noise file, its integration and its filtering using the exact same filter as we did for the old coil. Figure 2.8 show such a case of a noise file from the new coil recorded at the same sampling rate of 1 MHz.

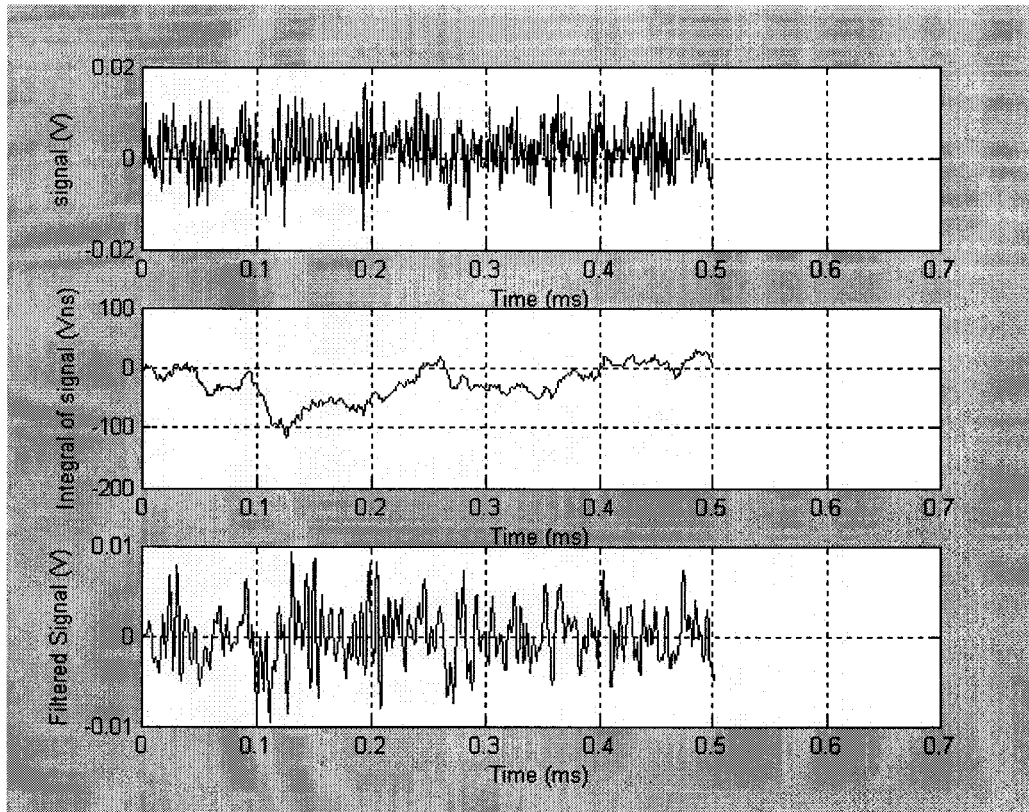


**Figure 2.8: Typical new coil noise file, its integration and its filtering.**

We verify once again that there is no trace of the low-frequency noise in the integrated signal. However, there is an oscillating frequency in the filtered signal. Could this be the 100 kHz low-frequency noise? Figure 2.9 shows the spectrum of the new coil filtered noise waveform, using FFT.

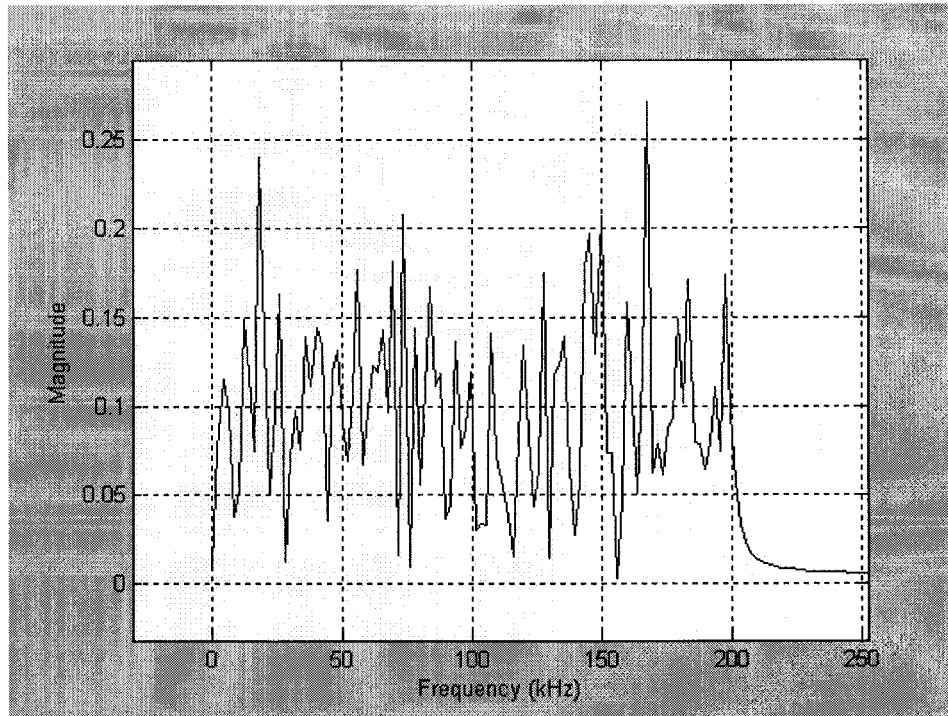


**Figure 2.9: FFT of a typical filtered noise waveform captured by the new coil.**

It is clear that there is no distinct peak at 100 kHz (compare with Figure 2.7), but rather a wide spectrum of frequencies without having a distinct peak. Hence, we conclude that the 100 kHz low-frequency noise is not traceable in the new coil signal.

The reader by now might wonder why this low-frequency noise, although quite small in amplitude, looks so big in the current and current derivative waveforms. If we recall Figure 1.10 we will see that the noise corresponds to a peak-to-peak amplitude of more than 2 kA at times. The reason for this is that the actual lightning signal when recorded, has also a quite small amplitude. The sensitivity of the old coil is  $359 \text{ mV/kA}/\mu\text{s}$ . This means that if there is a current flowing through the coil with an instantaneous derivative of  $1 \text{ kA}/\mu\text{s}$  the output of the coil will be only 359 mV. Furthermore, let us recall that the

old coil captures only one fifth of the current flowing through the tower. Thus the actual output of the sensing coil (when lightning strikes the tower) is usually in the magnitude of few hundreds of mV up to a few Volts. We can now see that the order of magnitude of the low-frequency noise is comparable to that of the actual lightning signal.

## **2.4 Existence of the Low-frequency Noise along the Tower's Structure**

A main concern of researchers working on the CN Tower lightning project has been whether the low-frequency noise is something related to the measurement system or an external signal picked up by the CN Tower. If it is an external signal picked up by the tower and flowing along the tower's structure, why is it not traceable in the new coil noise signal? In order to determine the source of this low-frequency noise, a visit was organized to the CN Tower's mast in order to test the new Rogowski coil located at the 509 m level above ground.

Before the planned entry to the CN Tower's mast we tried to answer the above mentioned question using clip-on current sensors and try to capture the noise at different locations, such as around one of the three conductors that extend from the lightning rods placed on the tower's tip to ground, the triax cable connecting the old Rogowski coil to the digitizer, etc. A handheld digitizer was used to record the signals. However, no definite conclusions were made since there was a lot of interference and we were not able to obtain stable signals.

As explained in Chapter 1, the new Rogowski coil utilizes an optical transmission system. The optical transmission system (NanoFast OP 2000A) consists of an optical transmitter that accepts  $\pm 1$  Volt full scale into 50 Ohms and an optical Receiver which provides  $\pm 1$  Volt out into 50 Ohms. The 3 dB bandwidth points are 35 Hz and 100 MHz. The input of the transmitter (located near the new coil at 509 m AGL) is connected to the new coil and the output of the receiver (located at the recording station at 403 m AGL) is connected to the digitizers. The fact that the optical transmitter accepts  $\pm 1$  Volt full scale necessitates the use of an attenuator since the output of the coil can reach voltages well above 1 Volt. (Recall that the new coil captures the whole lightning current derivative). The attenuator installed is a 30 dB, 20 Watt attenuator (RF-M3933/10-5). There was a thought that the use of the attenuator might be responsible for the complete absence of the low-frequency noise in the waveforms captured by the new coil.

It is worth mentioning that a visit to the CN Tower's mast, and especially to the location of the new Rogowski coil, requires a certain procedure including a lot of preparation. The coil is located in a restricted area where the radiated electromagnetic field is very high due to the presence of the transmitting antennas placed in the tower's mast. Thus, anyone visiting that area needs to be escorted by an expert and wear a full body-shielding suit that protects from the dangerous electromagnetic environment. In addition, the free space is very restricted and one can carry only a limited amount of equipment.

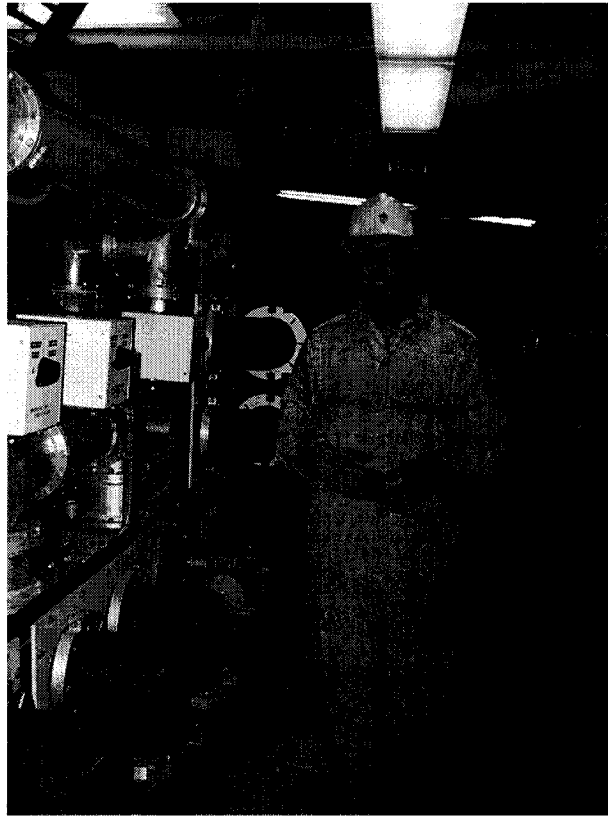


**Figure 2.10: CN Tower coil visit.**

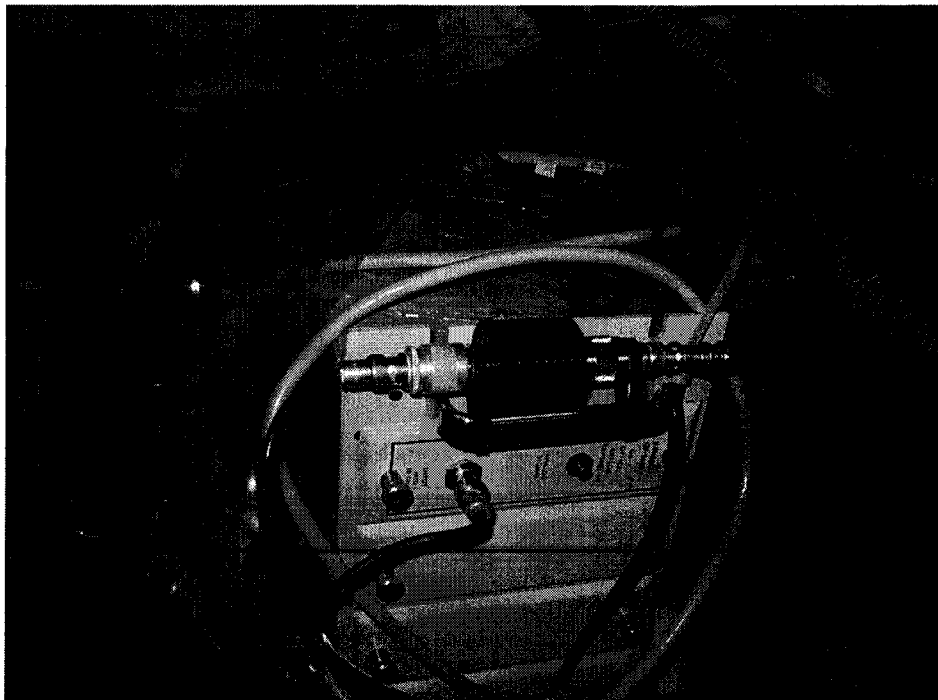


**Figure 2.11: Optical transmitter and attenuator at the new coil location.**

The main objective of the visit was to remove the attenuator and obtain noise files which would prove or disprove the existence of the low-frequency noise in the new coil signal. Figure 2.12 shows one of the waveforms obtained after the removal of the attenuator. This time the low-frequency noise appeared in the new coil waveforms and confirmed our speculations.

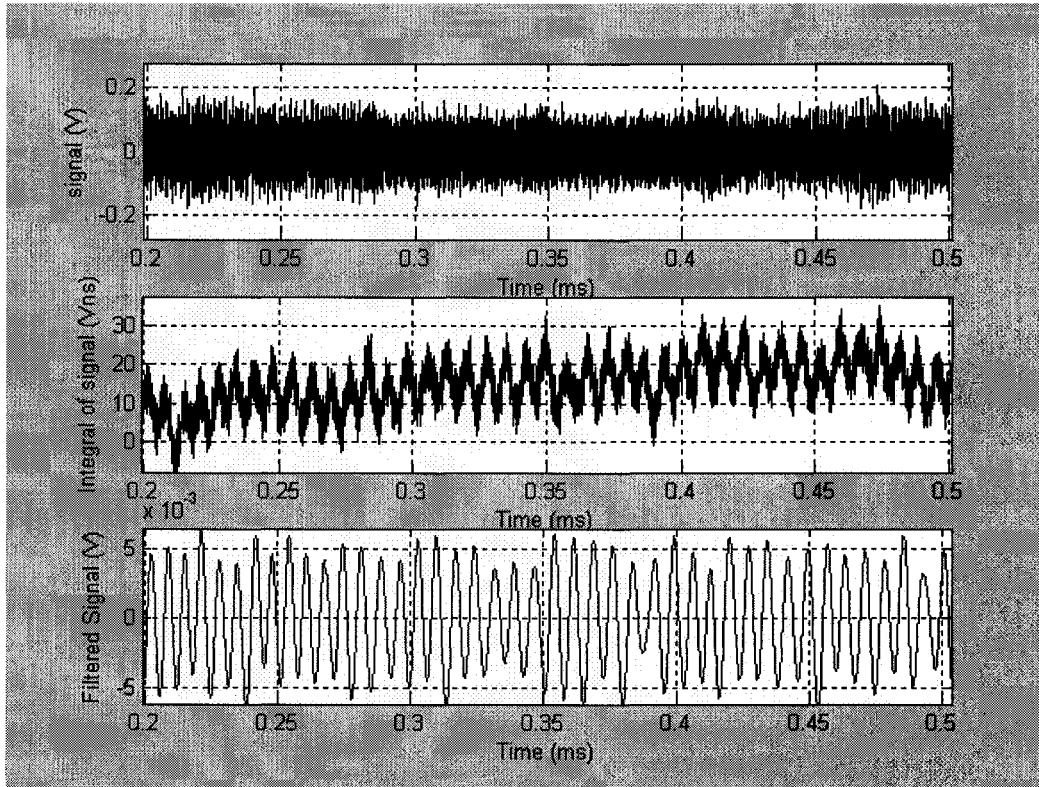


**Figure 2.12: New coil noise file captured after the removal of the attenuator.**

Figure 2.13 shows the spectrum of the filtered signal, which has now more pronounced peaks around 100 kHz.

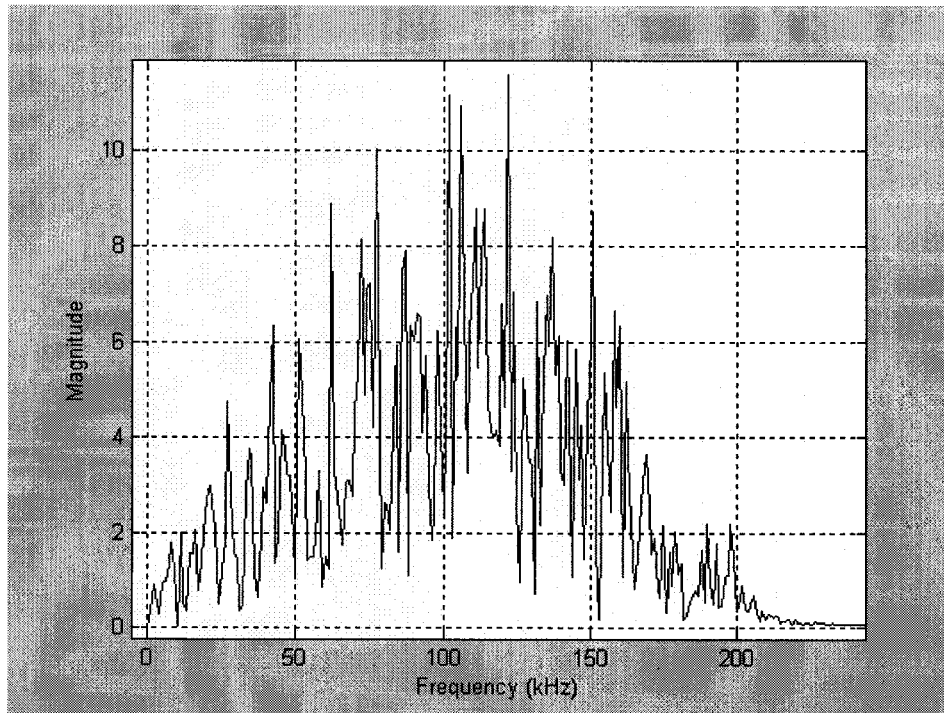


**Figure 2.13: FFT of a filtered noise waveform captured by the new coil, after the removal of the attenuator.**

The result of this test was a major contribution in the characterization of the low-frequency noise. Now we know that since the noise is captured by both the new and old coils, it must be an external signal picked up by the CN Tower's structure.

Figures 2.8 and 2.12 show that before the removal of the attenuator the peak-to-peak noise signal level was less than 40 mV whereas when the attenuator was removed the noise level reached 400 mV. The conclusion is that when the attenuator was used the low frequency noise was attenuated very much and became fully embedded in the high frequency noise. This explains why the low-frequency noise was not traceable in the new coil noise files. In addition, the usage of the optical transmission system doesn't add to

the noise captured by the new coil. The old coil however, utilizes a triax cable to connect the coil to the recording station. The length of this cable is more than 120 m and it is natural to be much more susceptible to interference. This is the reason that even after the removal of the attenuator the level of the low frequency noise is much less in case of the new coil than that for the old coil, although the new coil surrounds the whole structure.

During the CN Tower coil visit a calibration test of the attenuator was also performed. This was important because we need to know the exact value of attenuation in order to obtain correct values of the lightning current derivative captured by the new coil. The test was performed by transmitting a reference sinusoidal signal (800 mV, 100 kHz) from a function generator, through the optical transmission system, once with the usage of the attenuator and once without. Figure 2.14 shows the reference signal recorded by the LeCroy digitizer when transmitted directly through the optical transmission system (attenuator by-passed). Since a high frequency interference existed, the signal was filtered using a low pass filter.

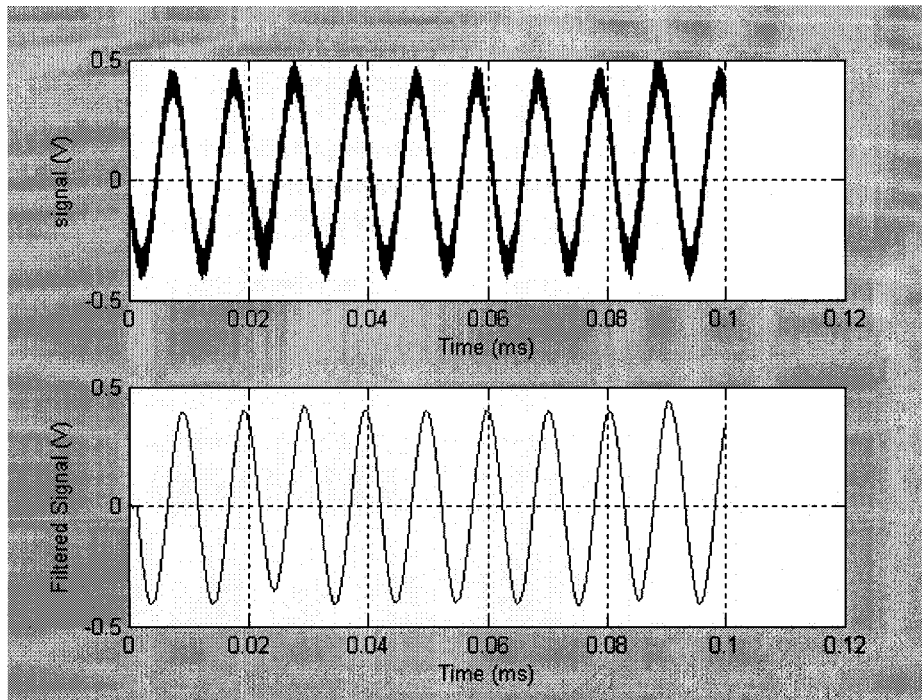


**Figure 2.14: Test signal without the attenuator.**

Then the attenuator was connected and the signal received at the recording station is shown in Figure 2.15.

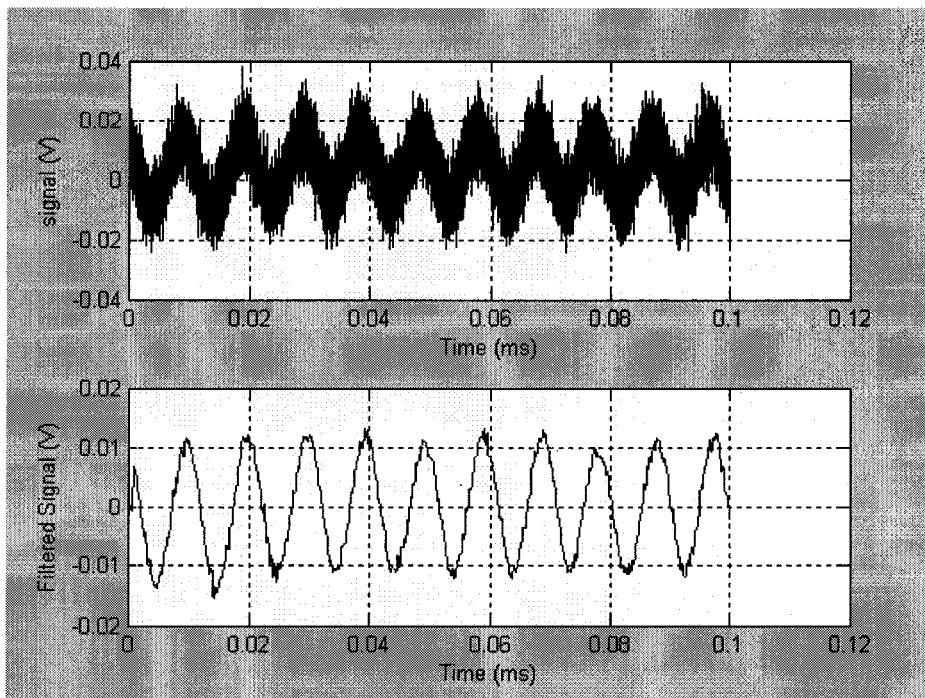


**Figure 2.15: Test signal with the attenuator connected.**

When the attenuator is connected the high frequency noise becomes much more dominant. This is also a proof that the source of the high frequency noise is not the CN Tower's structure, like the low-frequency noise, but rather an interference caused by the transmitting antennas in the mast. Because of the high frequency noise, filtering becomes a little problematic, however we can still measure the peak to peak amplitude of the noise signal with good accuracy. From the measurements we calculated the reference signal level to be 800 mV p-p before the connection of the attenuator and 20 mV p-p after the connection of the attenuator. This gives an attenuation factor of 40 times or 32 dB. There is a small decline between the measured attenuation (32 dB) and the theoretical one (30 dB) but this can be explained by the high frequency interference. The decision made was to use the theoretical attenuation of 30 dB.

## **2.5 Searching for the Source of the Low-Frequency Noise**

Once the major question of the nature of the noise was answered we started searching for the source of the noise. We referred to the Canadian Table of Frequency allocations and found out that a radionavigation system is using the frequency band of 90-110 kHz. After some more research we discovered that the radionavigation system using this band is called Loran-C.

# Chapter 3

## Loran-C

### 3.1 Introduction

Loran is an acronym for long-range navigation. It is a radionavigation system using land-based radio transmitters and receivers to allow mariners, aviators, and those interested in terrestrial navigation to determine their position. Loran-C transmitters are organized into chains of 3, 4 or 5 stations [22]. Within a chain one station is designated “Master” (M) while the other “Secondary” stations are identified by the letters W, X, Y and Z. The master station and the secondaries transmit radio pulses at precise time intervals. An on-board Loran-C receiver measures the slight difference in the time that it takes for these pulsed signals to reach the ship or aircraft from both master-secondary pairs. These time differences (TDs) are on the range of  $\mu\text{s}$ . Time differences for each master-secondary pair, are displayed by the mobile Loran receiver. The difference in the time of arrival of signals from a given master-secondary pair, observed at a point in the coverage area, is a measure of the difference in distance from the vessel to each of the two stations. The locus of points having the same TD from a specific master-secondary pair is a curved line of position (LOP). Mathematically, these curved LOPs are hyperbolas. With two or more lines of position, one can determine a fix (Using Loran-C overprinted maps). Each Loran-C chain provides signals suitable for accurate navigation over a designated geographic area termed a coverage area. The coverage areas of the various Loran-C chains overlap

somewhat and there are many areas in the United States and nearby coastal waters where two (or more) chains can be received and used for navigation. Currently there are 28 chains operating worldwide.

Loran-C transmitters vary in radiated power from less than 200 kW (kilowatts) to over 2 MW (megawatts). To lend some perspective, the radiated power output of a typical AM station in the United States might be 5 kW. For FM transmissions, the typical output would be larger, say 50 kW [22]. Exact comparisons of power output are difficult to make, because the Loran transmits only pulses. Nonetheless, in semi-quantitative terms at least, Loran transmitters are quite powerful. Among other factors, the radiated power controls the range at which a usable signal can be received and, therefore, the coverage area of the chain.

The transmitted signal consists of a series or group of pulses (each of a defined waveform). For the master signal, a series of nine pulses are transmitted (eight spaced 1000  $\mu$ s apart, followed by a ninth 2000  $\mu$ s later). (Pulsed transmission reduces the power requirements for system operation, assists signal identification, and enables precise timing of the signals.) Secondaries transmit a series of only eight pulses, each spaced 1000  $\mu$ s apart. This difference in the number of pulses, among other properties of the signal, enables Loran receivers to distinguish the signals from the master from those of the secondary stations (However, most receivers use phase codes for this purpose). The master and each secondary in the chain transmit in a specified and precisely timed sequence. First, the master station transmits. Then, after an interval sufficient to allow the

master signal to propagate throughout the coverage area, the first secondary in sequence transmits, and so forth. Normally, the secondary stations transmit in the alphabetical order of their letter designator. The secondary transmission is timed as follows: after the master signal reaches the next secondary in sequence, this secondary waits an interval, termed the secondary coding delay (SCD) or simply coding delay (CD), to transmit. The total elapsed time from the master transmission until the secondary transmission is termed the emission delay (ED). The ED is equal to the sum of the time for the master signal to travel to the secondary (termed the baseline travel time or baseline length (BLL)) and the CD. Next, other secondaries (each with a specified CD/ED) transmit in sequence. The sequence is completed when the master again transmits the nine pulse group.

The stations in the Loran chain transmit in a fixed sequence which ensures that TDs can be measured throughout the coverage area. The length of time in  $\mu\text{s}$  over which this sequence of transmissions from the master and the secondaries takes place is termed the Group Repetition Interval (GRI) of the chain. Since all Loran-C transmitters operate on the same frequency, the GRI is the key by which a receiver can identify and isolate signal groups from a specific chain. In naming the chains the GRI is included. For example the Great Lakes Chain has a GRI of 8970. This means the time interval between the pulse groups is 89700  $\mu\text{s}$ . The rightmost zero is always implied and the GRI is always in multiples of 10  $\mu\text{s}$ . Figure 3.1 shows the Loran-C pulse structure and sequencing for one chain. The master transmitter sends 9 pulses and then the secondaries follow with 8 pulses each. After the last secondary, the master transmits again. The GRI's and emission

delays are chosen in such way, that the pulses of one chain will never overlap in the chain's coverage area.

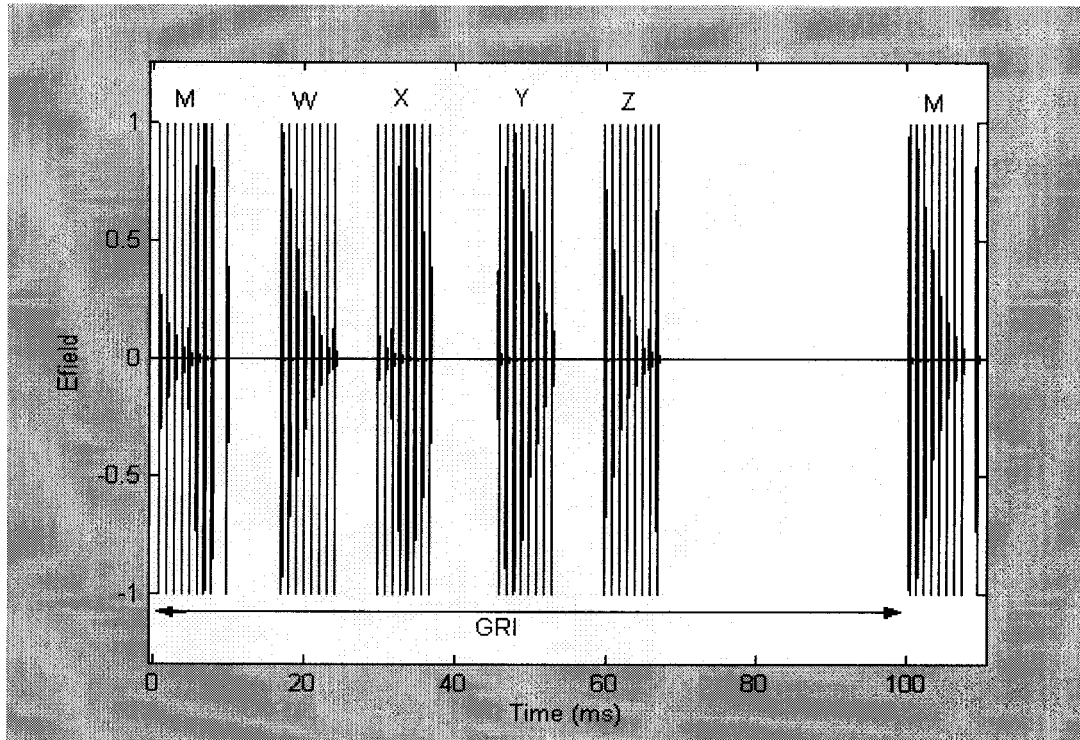


**Figure 3.1: Loran-C pulse groups and sequencing.**

Note: Although pulses look somewhat different in the figure, they are all identical. The reason for the different appearance is the compression done in the figure by Matlab in order to see a long time window.

Each station transmits signals, which have standard pulse leading-edge characteristics. Each pulse consists of a 100 kHz carrier that rapidly increases in amplitude in a prescribed manner and then decays at a rate, which depends upon the particular transmitter [23]. Each Loran-C pulse has an approximate duration of 200  $\mu$ s. Figure 3.2

shows the actual antenna current waveform for one pulse of a Loran-C signal and its frequency spectrum.

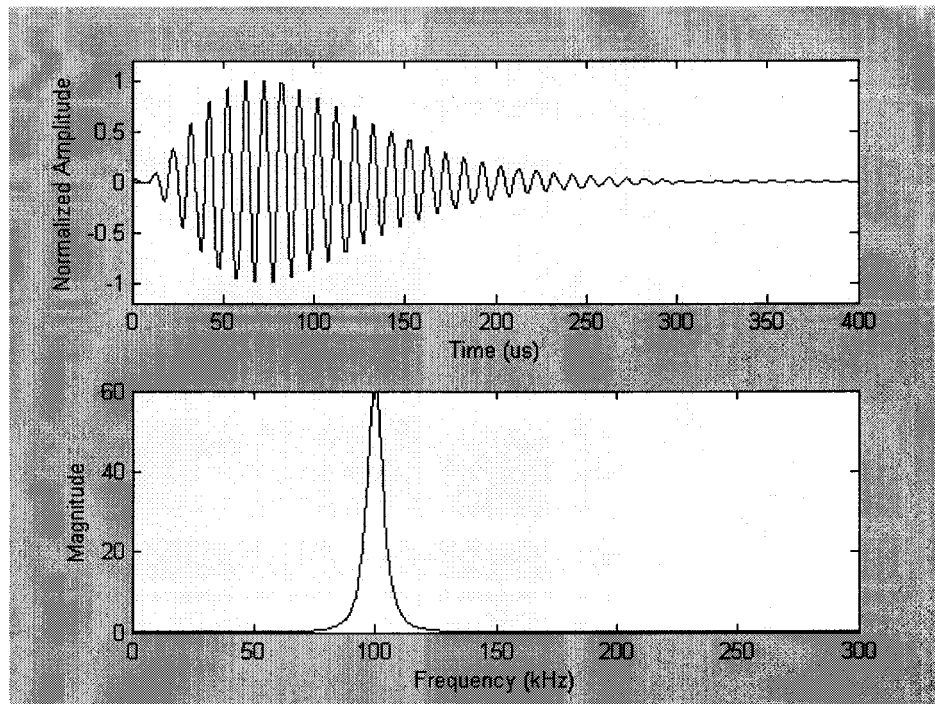


**Figure 3.2: Loran C pulse and its frequency spectrum.**

The pulse shape is designed so that 99% of the radiated power is contained within the allocated frequency band for Loran-C of 90 kHz to 110 kHz. This low frequency band was chosen for Loran-C primarily because it has relatively stable and predictable propagation characteristics and a fairly long range.

To provide contiguous service from one chain to the next, some stations are operated as members of two chains and radiate signals on two GRI's. In other words, some transmitters have only one function, meaning they serve only as a master or a secondary

in a particular chain, whereas others are dual rated, meaning that these can serve one function in one chain, and yet another in a neighboring chain. Such stations are periodically faced with the impossible requirement of radiating overlapping pulse groups simultaneously. To resolve this difficulty, one of the signals is blanked or suppressed during this time period. Dual rating is also desirable because it reduces the number of stations needed for coverage.

The transmitting antennas of the Loran-C system have a height of 200 m. As previously mentioned, the frequency used is 100 kHz, which corresponds to a wavelength of 3 km. Thus the antenna should ideally be 750 m for a  $\lambda/4$ -monopole antenna, but taking into consideration practical issues the decision was made to use 200 m monopole antennas. The receiving antennas are understandably much shorter, usually in the range of 2 to 3 m. Figure 3.3 shows a transmitting antenna used for Loran-C.

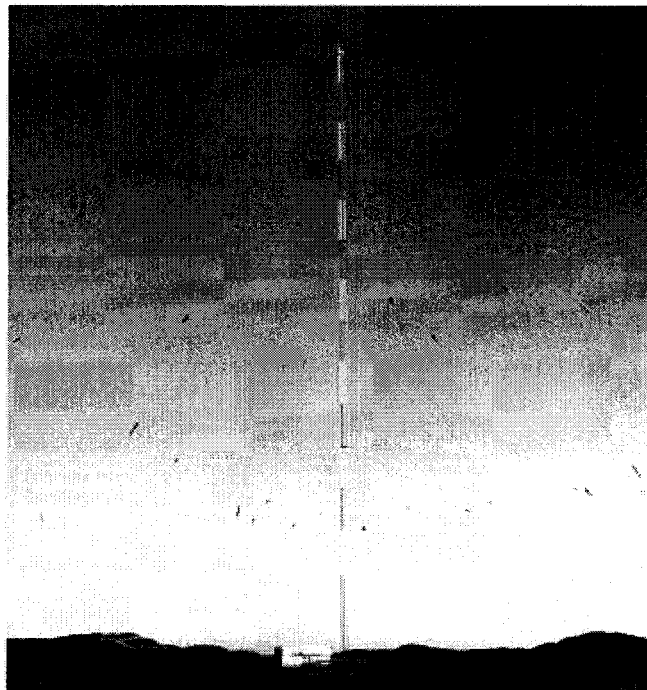


**Figure 3.3: Loran-C transmitting antenna.**

Although the Loran-C radionavigation system exists for a very long time now (45 years), we see nowadays a revival of the system in Europe, Russia and Asia [22]. The most important reasons for this revival are the fact that these countries do not want to become solely dependant on the satellite navigation system GPS, controlled by the USA, and that also in urban areas the 100 kHz signal penetrates better than the 1.5 GHz GPS signals.

Radio energy from a Loran-C transmitter radiates equally in the horizontal plane. The pulsed Loran-C signal, therefore, may reach the observer by many propagation paths. These paths are conveniently grouped into two major categories: (i) groundwave, and (ii) skywave.

### **3.2 Groundwave**

The groundwave signal propagates in the atmospheric medium in the vicinity of ground and is relatively well understood and quite predictable. However, the signal strength of the groundwave is attenuated as it follows the contour of the earth. At great distances from the transmitter, the groundwave signal is substantially attenuated. The amount of attenuation depends on the medium over which the groundwave propagates (seawater, fresh water, dry ground, wet ground etc), the frequency and the distance from the transmitting antenna.

### 3.3 Skywave

Skywaves consist of that component of the Loran-C signal that travels to the observer via reflection from the ionosphere, which is actually comprised of several reflecting layers, assigned letter symbols in conventional nomenclature. For the 100 kHz frequency of the Loran-C, this reflection takes place in the lower E or D region of the ionosphere. The effective reflection height varies from approximately 73 kilometers during daylight, to approximately 91 kilometers at night [24]. From the geometry of the reflection, it is obvious that the skywave signal must travel a longer distance to reach an observer and will arrive after the corresponding groundwave, generally after a time lapse of 35  $\mu$ s to 500  $\mu$ s (depending upon the height of the reflecting layer in the ionosphere). Figure 3.4 shows the path of the skywave from the transmitter to the receiver.

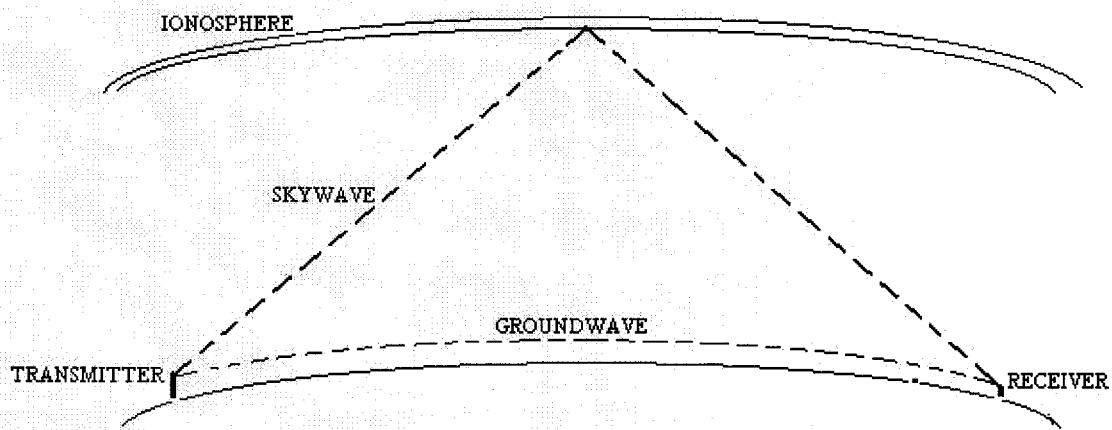


**Figure 3.4: Groundwave and Skywave paths.**

Skywave delay is the time difference, measured at the receiver, between the arrival of a point on the groundwave pulse from a transmitter and the corresponding point on the first skywave component. At short ranges the delay will be considerable, since the skywave pulse has traveled an additional distance of nearly twice the effective height of the ionosphere. The delay decreases as range increases.

From circular geometry it can be shown that the skywave delay is given by [24]:

$$t = \frac{2}{c} \left[ \left( h^2 + 4R(R+h) \sin^2 \frac{\beta}{2} \right)^{1/2} - R\beta \right] \quad (3.1)$$

where  $c$  is the velocity of EM waves ( $3 \times 10^8$  m/sec),  $h$  is the effective height of the ionosphere,  $R$  is the Earth's radius (6368 km) and  $\beta$  is equal to  $D/2R$  ( $D$  is the range from the transmitter to the receiver).

Figure 3.5 shows curves of skywave delay against range for typical daytime and nighttime effective ionospheric heights (73 km and 91 km respectively).

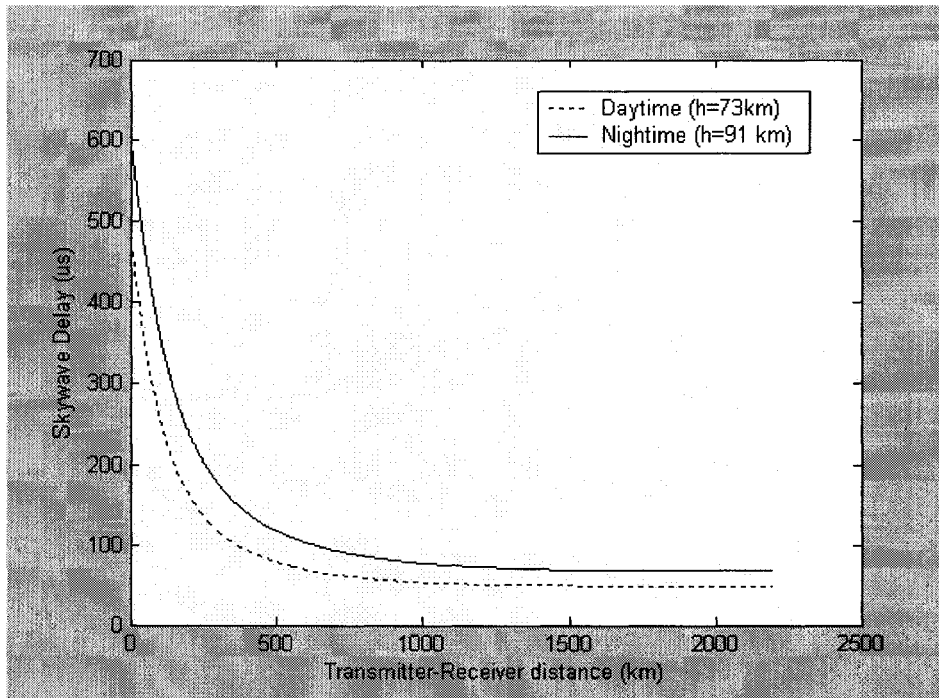


**Figure 3.5: Skywave delay vs range.**

Because skywaves do not travel over the surface of the earth, they are not attenuated to the same extent as the groundwave. In consequence, at long distances, the skywave signal may be very much stronger than the groundwave signal [24]. The skywave can cause distortion of the received groundwave signal in the form of fading and pulse shape changes, generally given the name skywave contamination.

Although it is possible to develop position information from skywave signals (and indeed, skywaves were used in early Loran), the most accurate navigation requires the use of the Loran groundwave [22]. The reason why groundwaves are preferred over skywaves for accurate navigation is that the propagation conditions (in the ionosphere) are not stable, but change from day-to-day and even hour-to-hour, which vastly complicates the problem of prediction of arrival times for skywaves. The skywave,

therefore, is generally regarded as a nuisance, and the Loran-C system has been designed in part to minimize the possible influence of skywaves on groundwave reception and tracking.

The Loran-C signal was designed so that the signal strength rises rapidly to maximum amplitude, reaching peak power early in the pulse and then gradually falls to zero. The rapid rise of the pulse allows a receiver to identify one particular cycle of the 100 kHz carrier. Cycles are spaced approximately 10  $\mu\text{s}$  apart. The third cycle of this carrier within the envelope is used when the receiver matches the cycles. The third zero crossing (termed the positive standard third zero crossing) occurs at 30  $\mu\text{s}$  into the pulse. This time is both late enough in the pulse to ensure an appreciable signal strength and early enough in the pulse to avoid skywave contamination from those skywaves arriving close after the corresponding groundwave.

### **3.4 Groundwave versus Skywave**

The Loran-C receiver is presented with the sum of skywave and groundwave. As we saw in the previous section the standard zero crossing precedes the earliest skywave component. Thus, the receiver makes its time measurement prior to the arrival of the skywave components. This protection against skywave interference is a major advantage of Loran-C over continuous-wave navigation aids. However, in practice, Loran-C receivers are limited in their ability to identify the standard zero crossing in the presence of strong skywave signals, especially those of short delay. The finite bandwidth of the

filters in a Loran-C receiver increases the risetime. The amplitude of the third cycle is greatly reduced. Actually, the narrower the filter, the greater the risetime and so the greater the susceptibility of the receiver to skywave interference. In practice, receiver designs are a compromise between filter bandwidth and skywave tolerance [25]. As we will clearly see in Chapter 4 it is very important to investigate what exactly is the groundwave to skywave ratio.

The groundwave field strength can be calculated analytically under the assumption that the transmitting antenna is a short monopole. If the length of a monopole antenna is smaller than one eighth of a wavelength (at 100 kHz,  $\lambda/8 = 375$  m), which is the case of a Loran-C transmitter (200 m tall), the current distribution is assumed to be linear,  $I_0$  at ground level and zero at the tip of the antenna. The amplitude of the electric field strength at the ground level a distance  $R$  from a monopole short antenna, placed above a perfectly conducting ground, is given by [26]:

$$E = (\eta / 4\pi R) \frac{2\pi}{\lambda} \ell I_0 \quad (3.2)$$

where  $\eta$  is the intrinsic impedance of free space ( $\eta = 120\pi$ ),  $I_0$  is the magnitude of the current at the terminal of the antenna and  $\ell$  is the length of the monopole antenna.

Substituting for the value of  $\eta$ , the amplitude of the electric field strength becomes:

$$E = \frac{60\pi}{R} \left(\frac{\ell}{\lambda}\right) I_0 \quad (3.3)$$

The total power radiated by such an antenna is easily determined [26]:

$$P = 20\pi^2 \left(\frac{\ell}{\lambda}\right)^2 I_0^2 \quad (3.4)$$

Using (3.3) and (3.4) a relationship can be developed relating the RMS value of the electric field ( $E_{RMS}$ ) to the total power radiated by the monopole antenna and the ground distance from the antenna to the point of observation (R).

$$E_{RMS} = \frac{300}{R} \sqrt{P} \text{ mV/m} \quad (3.5)$$

In the above expression the distance R is in kilometers and the power P is in kW.

Using Equation (3.5), Figure 3.6 shows the groundwave field strength in dB above 1  $\mu\text{V/m}$  for 100 kHz.

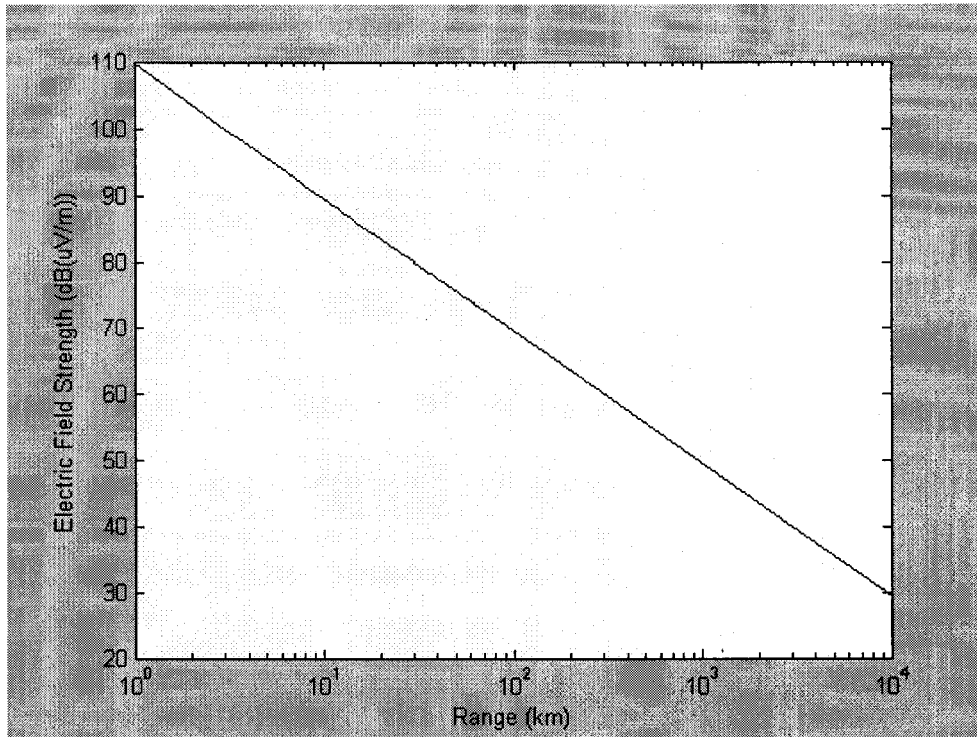


**Figure 3.6: Electric field strength for groundwave calculated analytically.**

The calculation of the electric field strength resulting from the skywave is somehow more complicated but we can estimate it using the following assumptions: The skywave propagates until it reaches the ionosphere following the same logic as the groundwave. Once it reaches the ionosphere it reflects and the wave becomes a plane wave propagating practically without attenuation until the receiver. Of course, we need to take into consideration the reflection coefficient of the ionosphere. The reflection coefficient of the ionosphere has been calculated to vary from 0.01 during the day to 0.25 during the night [24]. Under these rough assumptions, the RMS skywave field strength (nighttime) in dB above 1  $\mu\text{V/m}$  is shown in Figure 3.7.

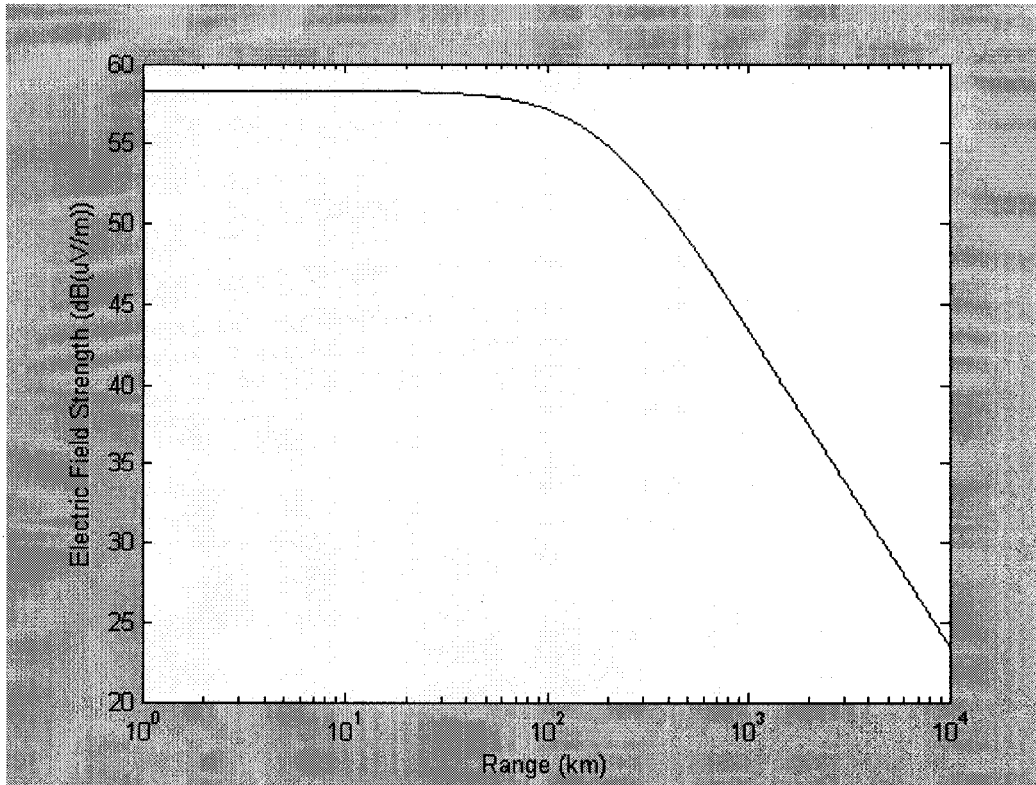


**Figure 3.7: Electric field strength for skywave calculated analytically (nighttime).**

Both groundwave and skywave field intensities as calculated above are not very accurate because they do not take into consideration the scattering caused by buildings and objects along the path of the groundwave as well as the highly unpredictable behavior of the ionosphere.

The International Telecommunications Union (ITU) has published groundwave propagation curves for frequencies between 10 kHz and 30 MHz taking into consideration all possible parameters [27]. Figure 3.8 shows the groundwave field strength for 100 kHz, 1kW transmitter power and land as the medium path.

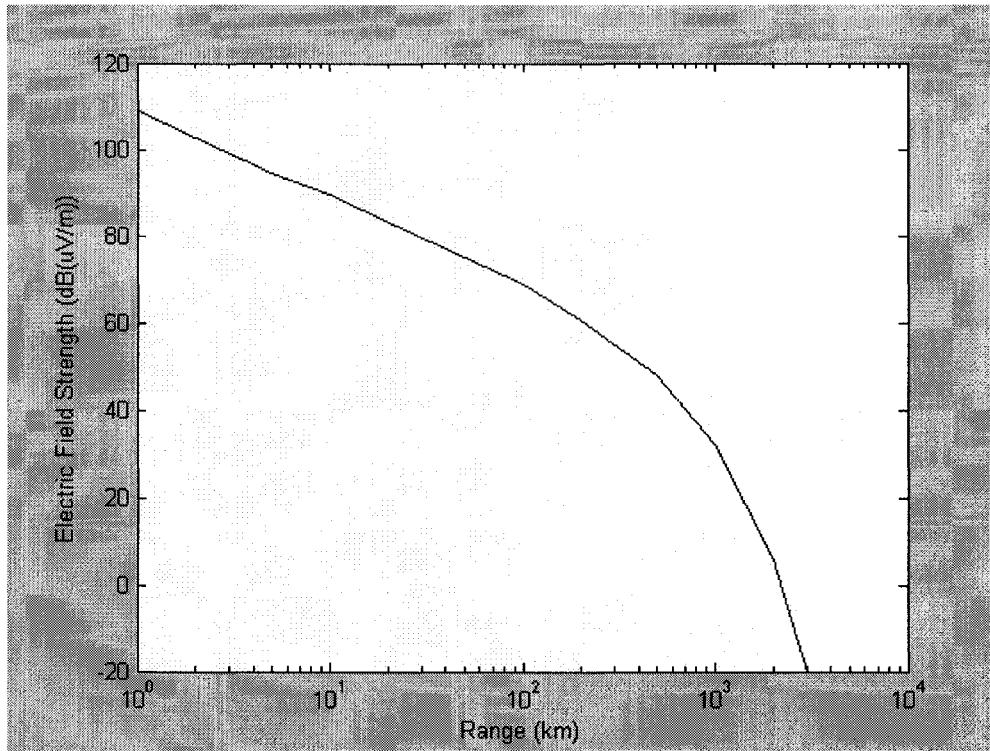


**Figure 3.8: Groundwave field strength for 100 kHz (ITU Recommendation P.368-7).**

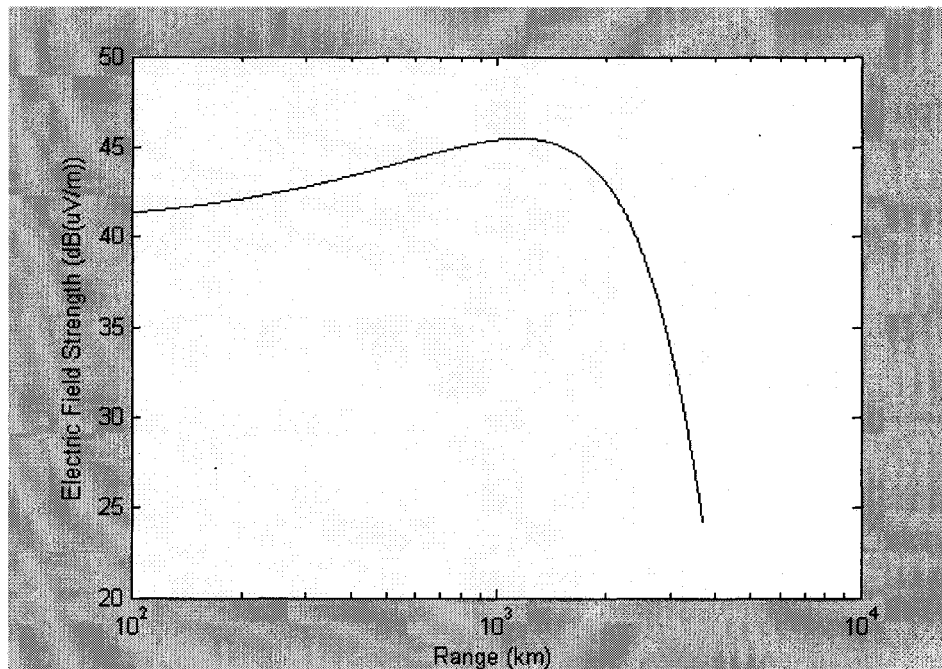
The US Coast Guard (USCG) has published curves of RMS skywave E-field strength at ranges of 1000 to 3700 km for night and day. The Decca Navigator Company has also published curves of skywave field strength for ranges of 100 to 500 km. Both publications are made by actual measurements of the field strength. When the Decca and USCG results are compared they correspond well with each other and so it is reasonable to produce a composite curve from the two sources by interpolating the gap. This composite RMS skywave field strength, in dB above 1  $\mu\text{V/m}$ , at a range of  $d$  km from a 1 kW transmitter has been fitted by means of the following polynomial [24]:

$$E = p_1 d^3 + p_2 d^2 + p_3 d + p_4 \quad (3.6)$$

**Table 3.1: Polynomial coefficients.**

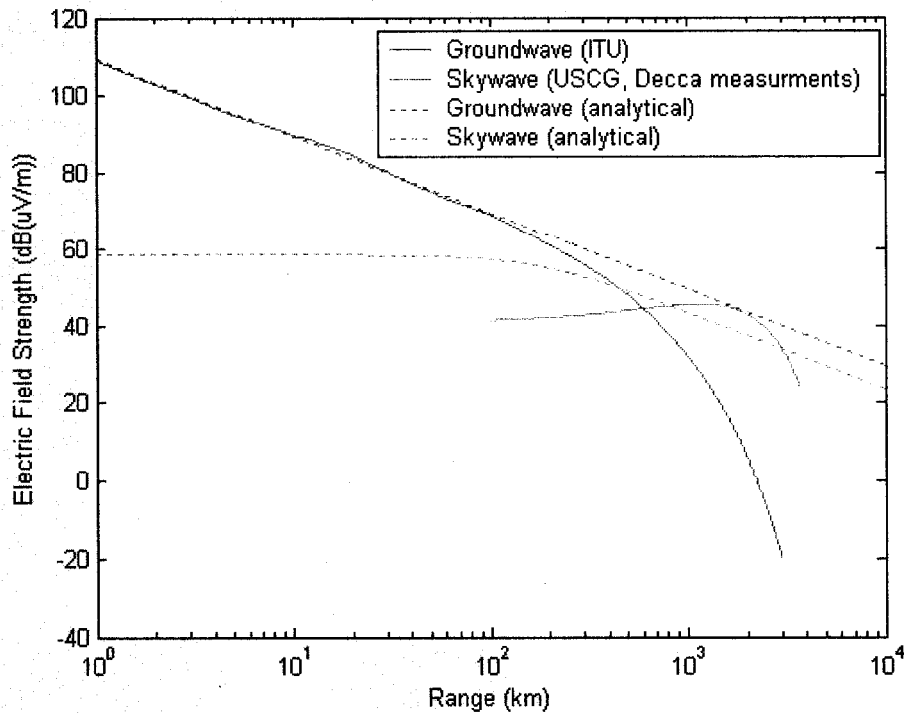
Time Period	$p_1$	$p_2$	$p_3$	$p_4$
Winter night	$1.2091 \cdot 10^{-10}$	$-4.0262 \cdot 10^{-6}$	$8.8139 \cdot 10^{-3}$	44
Summer night	$1.2091 \cdot 10^{-11}$	$-4.0262 \cdot 10^{-7}$	$8.8139 \cdot 10^{-3}$	40.5
Winter day	$5.4655 \cdot 10^{-12}$	$-8.4667 \cdot 10^{-8}$	$1.4137 \cdot 10^{-2}$	35

Figure 3.9 shows the composite skywave field strength using the polynomial given in Equation (3.6) for summer night. An interesting fact is that the skywave field strength actually increases for distances up to 1500 km.



**Figure 3.9: Skywave field strength for summer night.**

Previously we analytically computed both the groundwave and the skywave field strengths. This was the first step before using the more complex published curves which depend on actual measurements in case of the skywave. The comparison of the analytical computations versus the published ones is shown in Figure 3.10.



**Figure 3.10: Analytical vs published field strengths.**

From Figure 3.10, we observe that the groundwave computation is very accurate up to 100 km and after this distance the two results diverge. This divergence is expected since the scattering becomes larger with increasing distance and the attenuation factor is greater than  $1/R$ . The skywave curves are different but they are quite close in amplitude. The ionosphere has unpredictable behavior and that may explain the different shape. The above comparison was considered satisfactory and the decision was made to use the published curves for further computations.

For more clarity Figure 3.11 shows only the groundwave versus skywave field strength from the published curves.

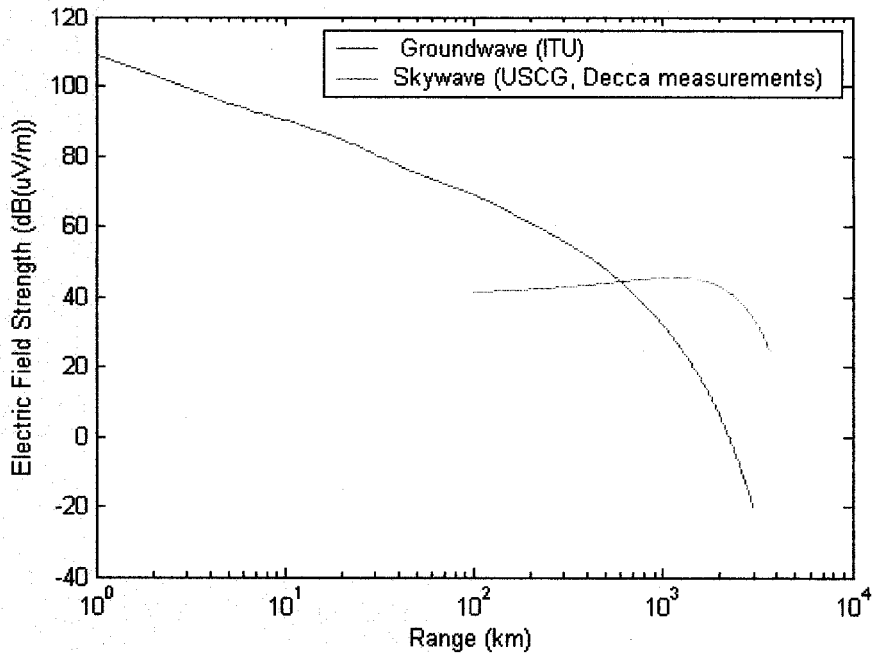


**Figure 3.11: Published field strengths for groundwave and skywave.**

As we will see in Chapter 4 it is very important to note that for distances greater than about 600 km, the skywave field strength is much stronger than the groundwave field strength.

### 3.5 The Electric Field of Loran-C

The principal transformation, which occurs between the antenna current and the far (typically greater than 5 to 10 wavelengths) E-field, is a 90° carrier phase shift [23]. The far E-field of the Loran-C pulse is described by:

$$e(t) = A \left( \frac{t}{\tau} \right)^2 e^{-2(1 - \frac{t}{\tau})} \cos(\omega t + PC) \quad (3.7)$$

where  $e(t)$  is the instantaneous value of the Electric field

$A$  is a constant that corresponds to the maximum value of the field.

$t$  is the time in  $\mu\text{s}$

$\tau$  is a time constant ( $\tau = 65 \mu\text{s}$ )

$\omega = 200\pi \text{ kr/s}$

PC is a phase code (0 or  $\pi$ )

Figure 3.12 shows the far electric field for a train of pulses of a master station and the corresponding spectrum.

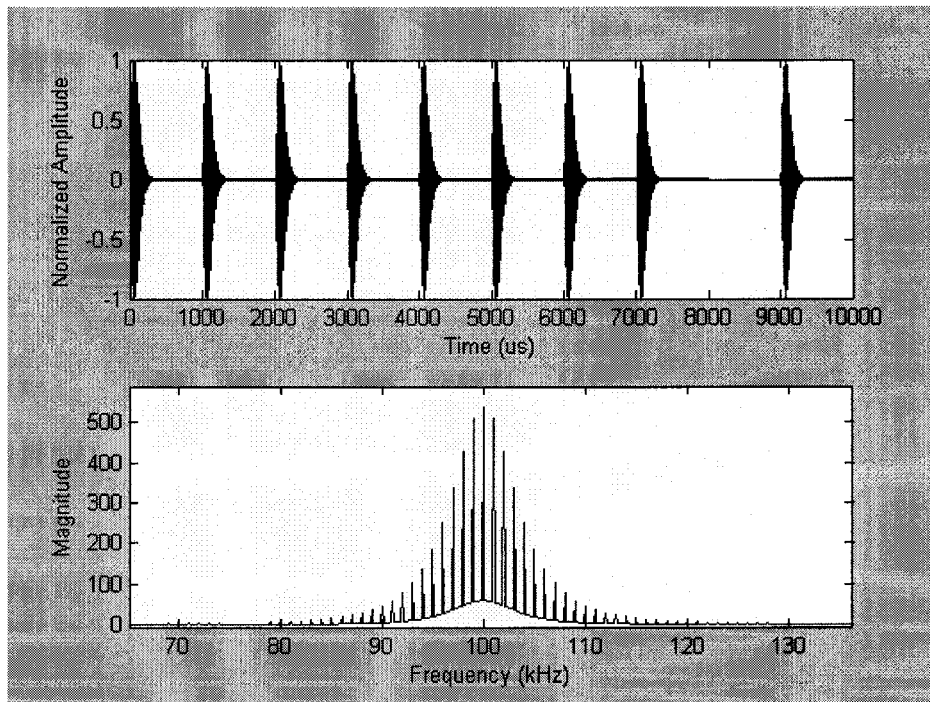


**Figure 3.12: Electric field for a master station pulse group and its spectrum.**

# Chapter 4

## The CN Tower: A Receiver of Loran-C

### 4.1 Lightning as Noise for Loran-C

Before we delve into the main issue of this chapter, we shall take a look into a very interesting topic. Atmospheric conditions can significantly affect the received Loran-C signal, and consequently the accuracy of the obtained fix [22]. Atmospheric noise is the dominant form of noise in the Loran band. It is produced by lightning all over the earth. Atmospheric noise is always present, because thunderstorms are always present at various places. It is estimated that globally about 100 lightning flashes occur each second which translates into close to 10 million flashes per day [1]. Each lightning strike produces a point noise source. The effects of this noise depend upon the distance from the storm to the receiver. Atmospheric noise is generally greater in the summer than the winter, and in the tropics compared to the higher latitudes. Therefore, although it is known that lightning is the main source of noise for the reception of Loran-C, it will be shown that the Loran-C signal is the main source of noise for the measurements of lightning current at the CN Tower. The figure shows a Loran-C transmitting station in Malone, Florida, with lightning in the background.

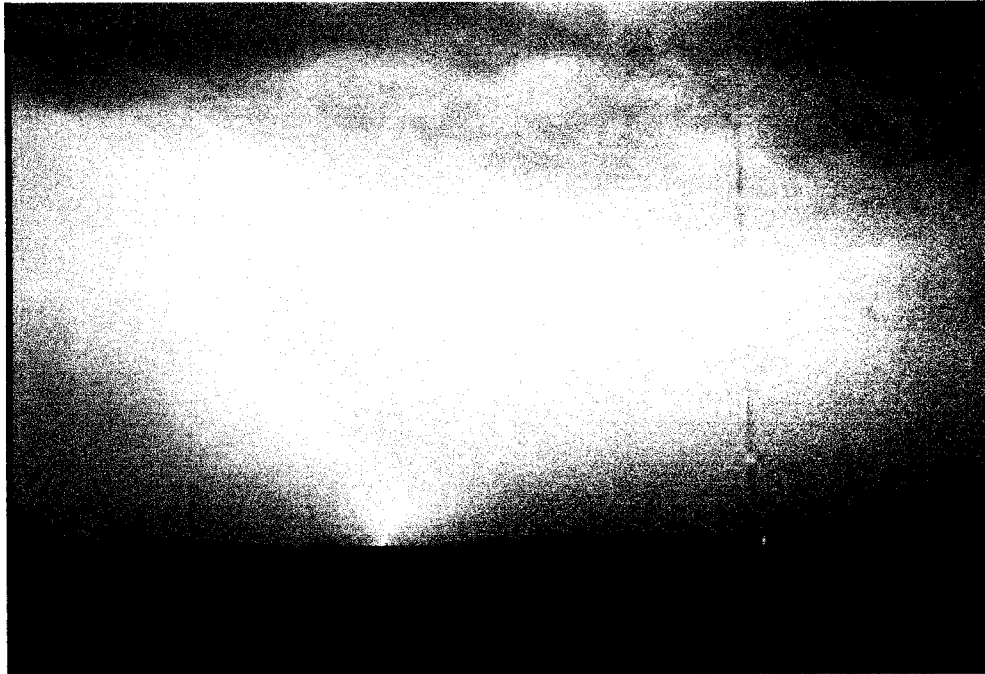


**Figure 4.1: Loran-C transmitting antenna in Malone, with background lightning.**

This fact shows again that lightning and Loran-C signals share a certain frequency band and makes this research more valuable since Loran-C researchers can obtain valuable information on the effect of lightning in the transmission of Loran-C signals.

#### **4.2 Is the CN Tower an efficient receiving antenna for Loran-C?**

In order to assess correctly if the received low-frequency noise is in fact the Loran-C signal we first have to answer the question if the CN Tower is an efficient antenna for this frequency. As we saw in Chapter 3 the frequency of 100 kHz used for Loran-C results in a wavelength of 3 km. The most efficient monopole antenna for this frequency would be a  $\lambda/4$  m monopole antenna of 750 m. The CN Tower at a height of 553 m above

ground level, provides an almost perfect antenna for this frequency considering its metallic and steel inforced structure. The efficiency of the CN Tower as a receiving antenna for Loran-C is much higher than even the transmitting antennas of Loran-C which are “only” 200 m tall. Very important is the fact that the polarization of the Loran-C wave (the direction of the E-field) is vertical which means that the CN Tower will indeed act as an efficient receiving antenna. Furthermore, the fact that the CN Tower rises much above all other buildings and structures in its vicinity and in the Greater Toronto Area, makes it even more efficient as a receiver of Loran-C signal. It has become obvious by now, that the possibility of the received signal being the Loran-C signal is extremely high.

### **4.3 Motivation for Composing the Loran-C Signal at the Location of the CN Tower**

The main remaining unanswered question is why we always observe the noise signal in our limited time records whereas Loran-C is a pulsed transmission system. It was thought that maybe the pulses from different stations of different chains overlap somehow and produce a composite signal that is always present. However, the long time interval between pulses and pulse groups, made this hard to understand. Therefore, a thorough attempt was made to simulate the electric field Loran-C signal as received at the CN Tower, taking into consideration as many parameters as possible.

#### 4.4 Loran-C Stations “Close” to the CN Tower

We first examined which Loran-C stations are located close enough to the CN Tower and have a strong effect in the reception of Loran-C signal. Figure 4.2 shows the Loran-C transmitting antennas located in North America. The stations that are considered close enough and used for the following computations are the ones that are indicated by their names in Figure 4.2. The station located north of Carolina Beach (Wildwood New Jersey, purple color) is an experimental station. We can also see the control stations which monitor the proper operation of the system.



Figure 4.2: Loran-C Stations “close” to Toronto.

Out of the nine stations taken into consideration, eight of them are assigned as dual rated. Recall from Chapter 3 that this means that they are used for two different chains, transmitting signals in two different GRI's. Table 4.1 summarizes the use of each station according to the chain it belongs and its function in that chain. (Master or Secondary).

**Table 4.1: Loran-C stations close to Toronto and their functions.**

Loran-C Station	Function 1	Function 2
SENECA	Master for 9960	Secondary for 8970
CARIBU	Secondary for 9960	Master for 5930
NUNTUCKET	Secondary for 9960	Secondary for 5930
CAROLINA BEACH	Secondary for 9960	Secondary for 7980
DANA	Secondary for 9960	Master for 8970
COMFORT COVE (single rated)	Master for 7270	
CAPE RACE	Secondary for 7270	Secondary for 5930
FOX HARBOR	Secondary for 7270	Secondary for 5930
BAUDETTE	Secondary for 8290	Secondary for 8970

The stations of Seneca, Caribu, Nuntucket, Carolina Beach and Dana comprise the 9960 Northeast U.S. Loran-C chain which is the closest one to Toronto and would be used from a Loran-C user in this area. The stations of Comfort Cove, Cape Race and Fox Harbor comprise the 7270 Newfoundland East Coast Loran-C chain. The other functions of these stations are shown in the above table. Finally the station of Baudette belongs to both the 8290 North Central U.S. Loran-C Chain and the 8970 Great Lakes Loran-C Chain.

The coordinates of the CN Tower location are:  $43^{\circ} 38' 36''\text{N}$  and  $79^{\circ} 23' 15''\text{W}$ . These coordinates were obtained by the use of a handheld GPS navigator at the CN Tower. The coordinates of each Loran-C station are published in the US Coast Guard publication: "Specification of the transmitted Loran-C signal" [23]. The distance between each station and the CN Tower was calculated using the on-line application of the Geodetic Survey Division for Geographic Inverse Computation (Natural Resources Canada) [28]. Then, the time delay of each station to the CN Tower was calculated. It was assumed that the speed of the transmitted signal is the speed of light.

The US Coast Guard also publishes the Emission Delay of each station. We recall that the emission delay is equal to the time it takes for the signal to travel from the master station to a secondary station plus the predefined coding delay. Hence, since the instant a master station transmits a pulse this pulse will reach the CN Tower after the time specified by the distance of the station to the tower, and the subsequent pulses of the other stations in the same chain will reach the CN Tower after a time delay equal to the Emission Delay plus the delay of each station to the CN Tower. We refer to this time delay as the total delay.

The skywave delay time was calculated for each station according to the distance of the station to the CN Tower and as described in Section 3.3. Calculations for the skywave delay were made for both daytime and nighttime.

The groundwave and skywave field strengths resulting from each station, as received at the CN Tower was calculated using Figure 3.11. However, the electric field intensities were calculated in  $\mu\text{V}/\text{m}$  instead of dB above  $1 \mu\text{V}/\text{m}$ . The latter unit was used in Figure 3.11 as it provides a better understanding of the image. The skywave field strength was obtained for both daytime and nighttime.

All the above calculations are shown in Table 4.2. Because of the fact that most of the stations are dual rated, we calculated the total delay twice: once for each function of the station as described in Table 4.1 (Emission Delays do not apply to master stations). Finally the power of each transmitting station is also included in the table.

**Table 4.2: Comprehensive table of stations close to Toronto.**

STATION	LOCATION	DISTANCE TO CN TOWER (m)	DELAY TO TOWER (µs)	ED (µs)		TOT. DEL.		ED (µs)		TOT. DEL. FUN. 2 (µs)	SKYWAVE DEL. DAYTIME (µs)	SKYWAVE DEL. NIGHTTIME (µs)	POWER (kW)	E-FIELD (µV/m)	
				FUN. 1	FUN. 2	FUN. 1	FUN. 2	FUN. 1	FUN. 2					GROUNDWAVE	SKYWAVE (DAY)
SENECA	42° 42' 50.716"N	232445	775	N/A	775	31162.06	31937	143.9	213.6	800	549	141	211		
	76° 49' 33.308"W														
CARIBU	46° 48' 27.305"N	965239	3217	13797.2	17014	N/A	3217	54	78.4	800	32	187	280		
	67° 55' 37.159"W														
NUNTUCKET	41° 15' 12.046"N	817871	2726	26969.93	29696	13131.68	15858	58	85.2	400	52	183	275		
	69° 58' 38.536"W														
CAROLINA BEACH	34° 03' 46.17"N	1071216	3571	42221.65	45793	61542.72	65114	52.2	75.2	600	22	188	282		
	77° 54' 46.21"W														
DANA	39° 51' 7.658"N	793901	2646	57162.06	59908	N/A	2646	58.8	86.6	400	57	182	273		
	87° 29' 11.586"W														
COMFORT COVE	49° 19' 53.57"N	1976093	6587	N/A	6587	N/A	6587	48.9	67.9	250	2	133	200		
	54° 51' 42.57"W														
CAPE RACE	46° 46' 32.286"	2078565	6927	12037.49	18964	28755.02	35682	48.9	67.9	500	1	124	185		
	53° 10' 27.606"														
FOX HARBOR	52° 22' 35.252"N	2002913	6676	26148.01	32824	41594.59	48271	48.9	67.9	900	1	131	196		
	55° 42' 27.862"W														
BAUDETTE	48° 36' 49.947"N	1292905	4310	14786.58	19097	47753.74	52064	50	71	800	12	184	275		
	94° 33' 17.915"W														

## 4.5 Composition of Loran-C at the Location of the CN Tower

After the calculation of all the above parameters the simulation of the Loran-C signal as received at the CN Tower was possible. Because of the variation in the height of the ionosphere during the day, calculations were made for both daytime and night time. The power of each station was taken into consideration using the relation between field strength the radiated power as shown in section 3.4.

First let us see how the Loran-C signal is received at the location of the CN Tower for only one chain Figure 4.3 shows the electric field of the 9960 chain which is the most dominant near the CN Tower for daytime.

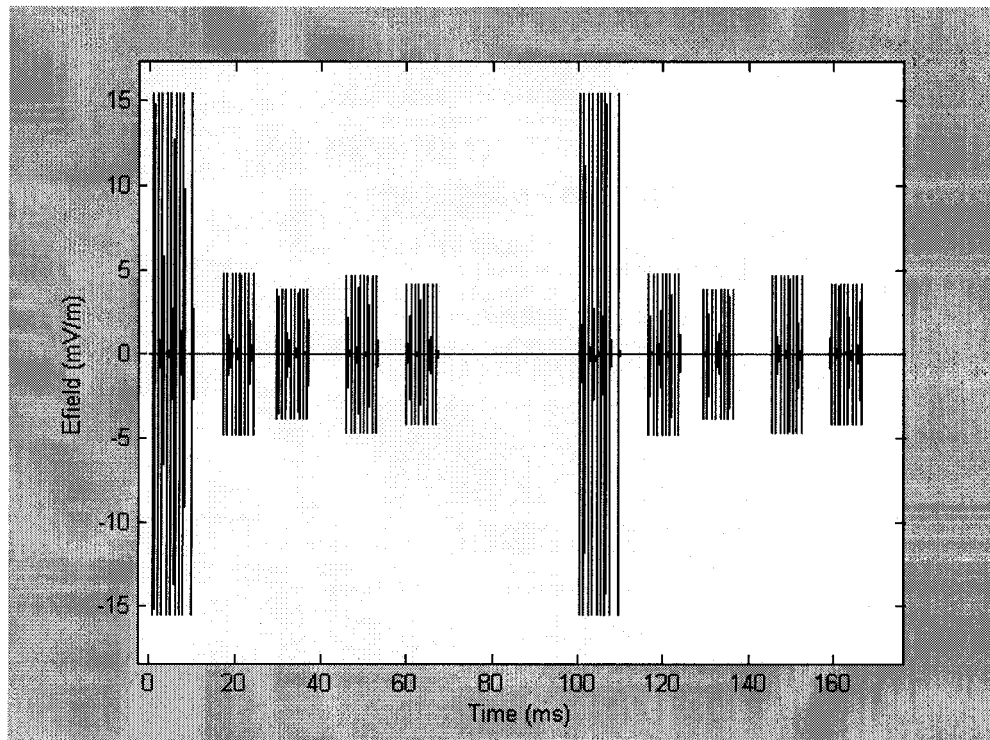


**Figure 4.3: Electric field of 9960 chain at the location of the CN Tower for daytime.**

The figure shows the electric field strength for 2 GRI's. The first pulse group corresponds to the Seneca station and has the highest amplitude since it is very close to the CN Tower (232 km). The subsequent pulse groups correspond to the stations of Caribu, Nuntucket, Carolina Beach and Dana, respectively. Afterwards, the pattern repeats again. We can now notice that the pulses do not overlap, which is expected, since the Coding Delay of each station was chosen according to that principle. In order to obtain a clear picture, let us zoom in one pulse. Figure 4.4 shows the very first pulse of the Seneca station for daytime.

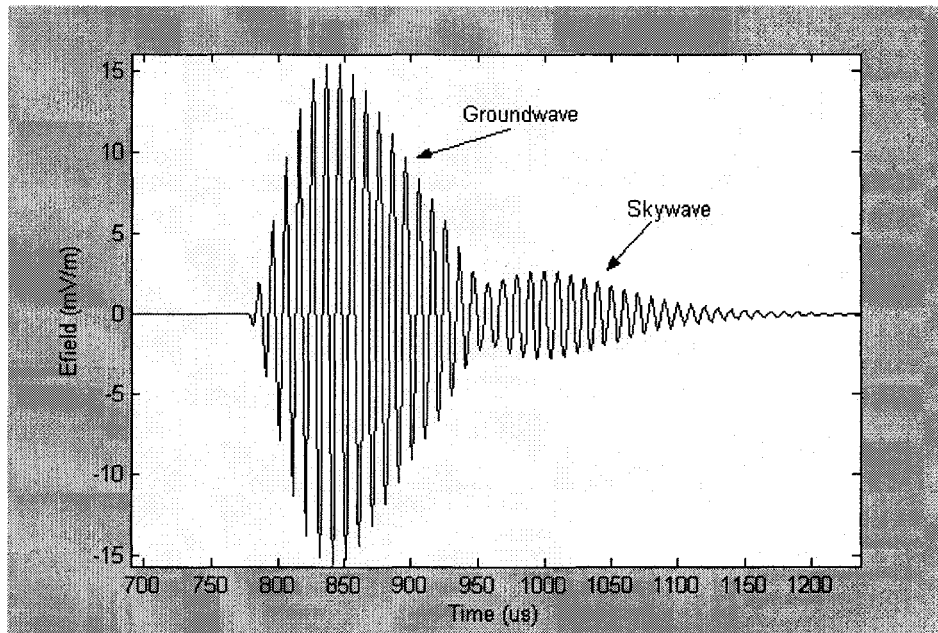


**Figure 4.4: Electric field strength of one Seneca station pulse for daytime.**

The pulse reaches the CN Tower 775  $\mu\text{s}$  after its transmission. We can clearly see the skywave reaching the CN Tower 141  $\mu\text{s}$  after the groundwave. In this case the skywave is relatively weak compared to the groundwave, because the Seneca station is close to

Toronto and hence, the groundwave field strength is much higher than the skywave field strength while the pulse shown in Figure 4.4 is for daytime. Figure 4.5 shows the exact same pulse but for nighttime.

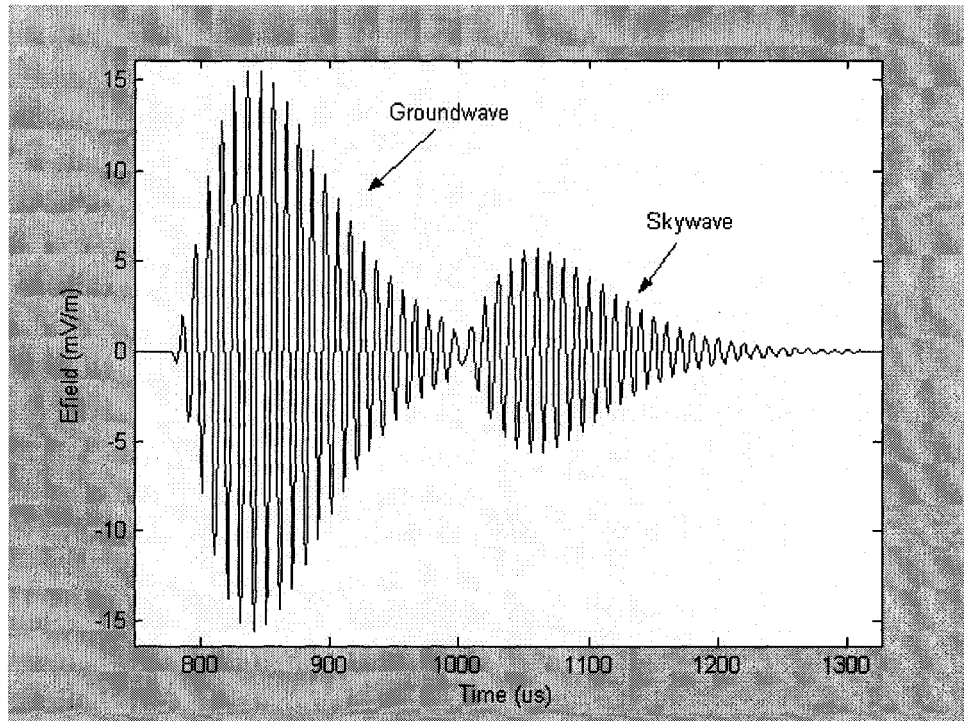


**Figure 4.5: Electric field strength of one Seneca station pulse for nighttime.**

The skywave in this case appears stronger but because of the short distance it is still substantially weaker than the groundwave. Nonetheless, in both cases the skywave has a big effect on the received pulse since it spreads out in time.

Now we will take a look into the pulse shape of the Caribu station (located 965 km away from the CN Tower) in order to investigate the behavior of a relatively far station. Figure 4.6 shows the first pulse of the Caribu station as received at the Tower.

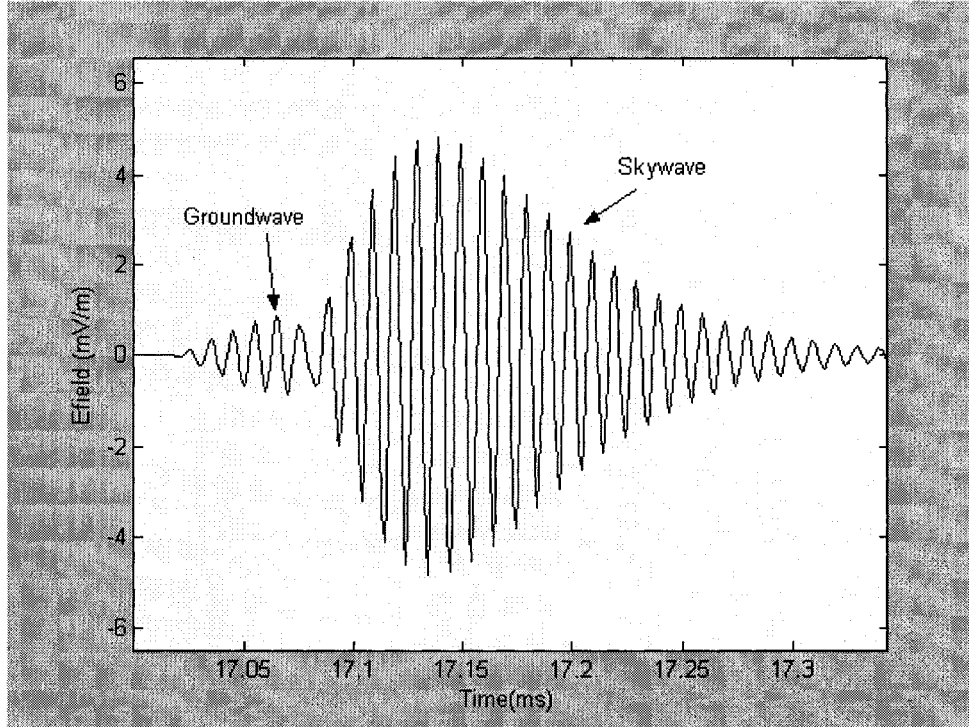


**Figure 4.6: Electric field strength of one Caribu station pulse for daytime.**

In this case the skywave arrives very soon after the groundwave (because of the large distance) but the strength of the skywave is much higher than that of the groundwave even for daytime. In fact, the groundwave is almost negligible compared to the skywave. During the nighttime the skywave is even stronger. Figure 4.7 shows the same pulse when received at nighttime.

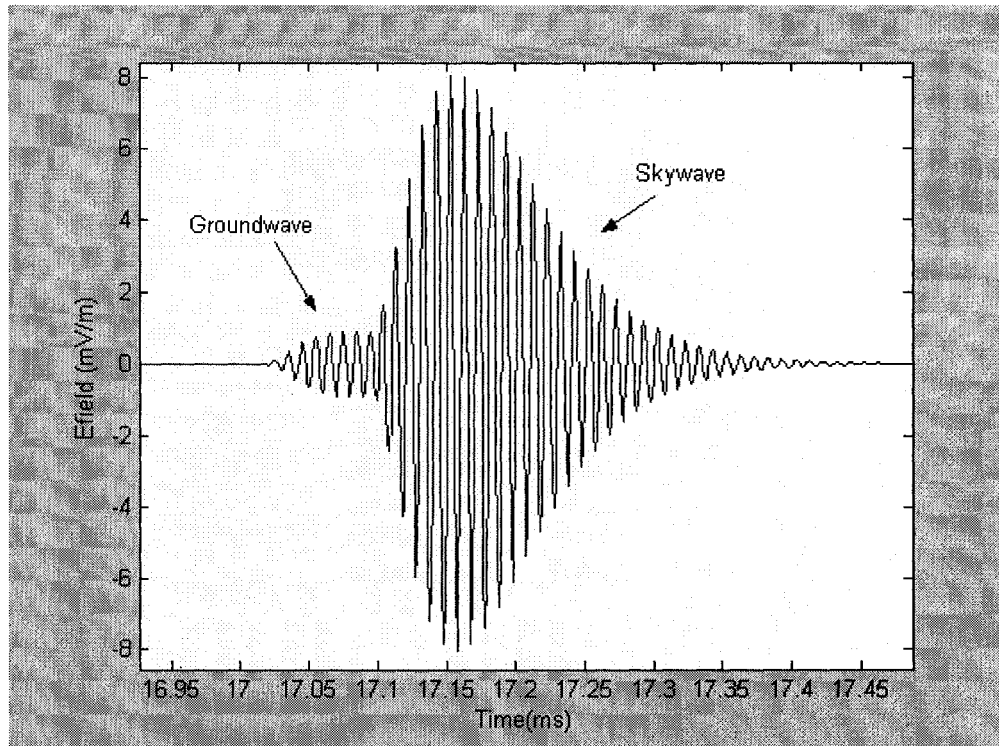


**Figure 4.7: Electric field strength of one Caribu station pulse for nighttime.**

The skywave is even stronger now. The above figures illustrate the importance of skywave in the reception of Loran-C.

Simulations for the 7270 chain and the 8290 chain (including only the Baudette station) were done in a similar way. We then computed three more simulations for the same nine stations but this time they were considered as stations of the other chains they operate in, using different GRI's according to Table 4.1. All the resulting signals were added composing a final signal of the Loran-C signal as calculated at the location of the CN Tower. We have to make it very clear at this point, that because of the different GRI's the time delay between different groups will always change generating an unlimited number of possible combinations. Thus, the composite result shown below is only one possible

scenario out of the unlimited number of combinations. The electric field at the location of the CN Tower due to each of the stations is shown in Figure 4.8. Different colors represent different chains.

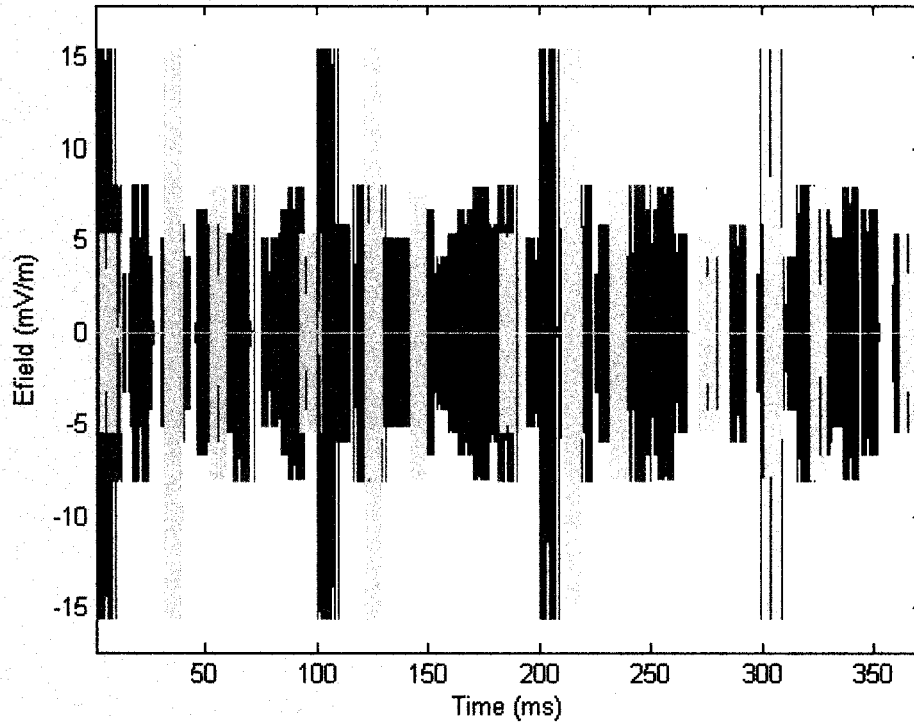


**Figure 4.8: Electric field calculated at the location of the CN Tower due to each of the stations of table 4.2 for nighttime.**

We can now see clearly that the superposition of all the signals produces a composite signal that is present most of the time. We can also see the addition of the signals over a short time window in order to appreciate the result better. A random portion of the composite signal obtained by addition is shown in Figure 4.9.

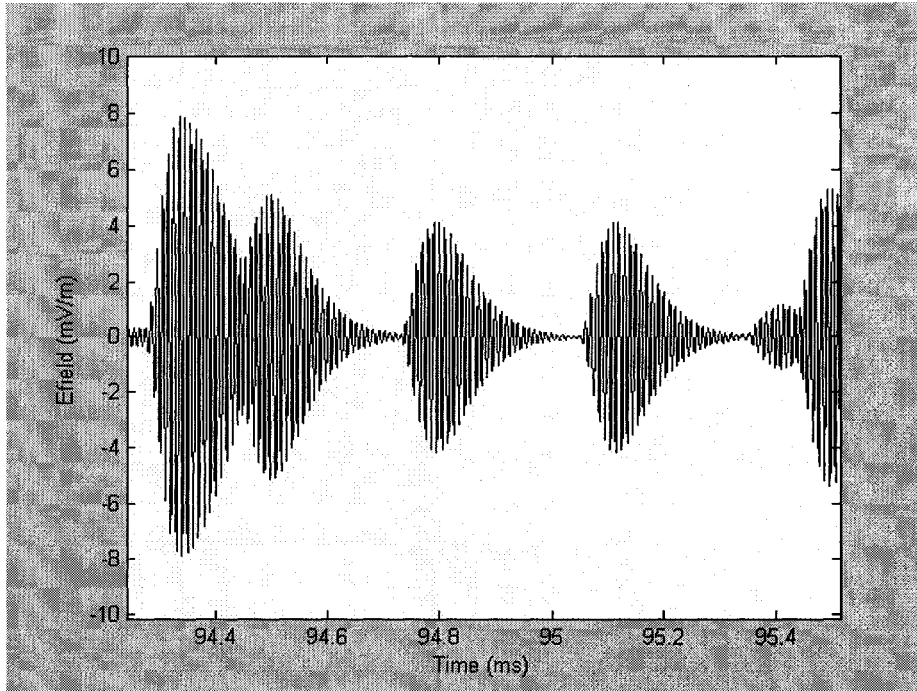


**Figure 4.9: Composite signal of the electric field of Loran-C at the CN Tower for nighttime.**

The spectrum of the composite signal using FFT is shown in Figure 4.10.

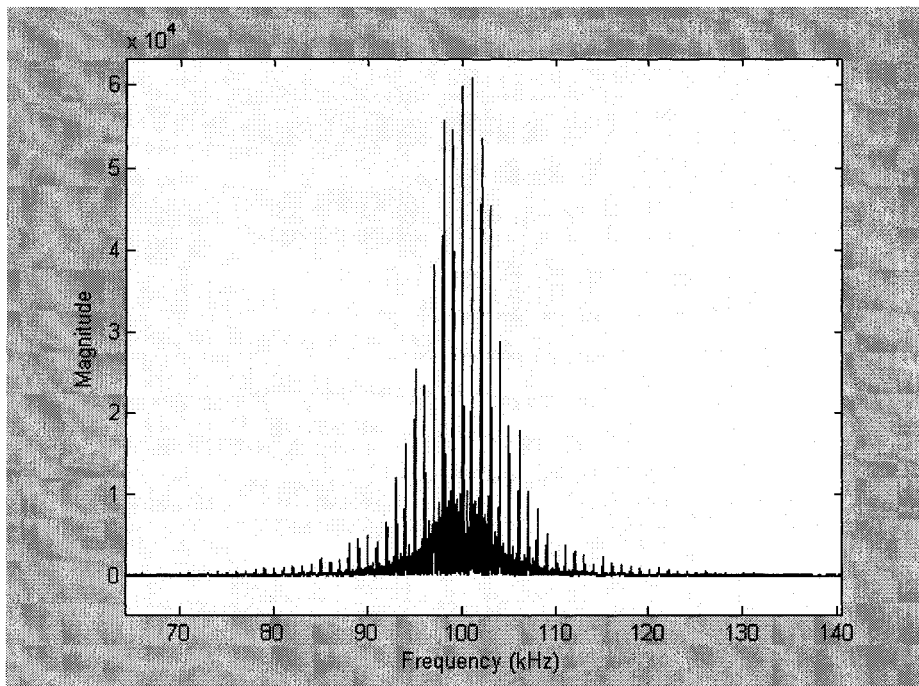


**Figure 4.10: Spectrum of simulated Loran-C signal at the CN Tower.**

During the last stages of the thesis work there was some communication with Mr. Poul Henning Kamp from Denmark. Mr. Kamp has been doing Loran-C related research over the past few years. Figure 4.11 shows a sample of a signal he recorded in Europe using a Loran-C receiver. Figure 4.12 shows another noise signal that we recorded at the CN Tower. The apparent resemblance adds to the confirmation that the low-frequency noise received at the CN Tower is the Loran-C signal.

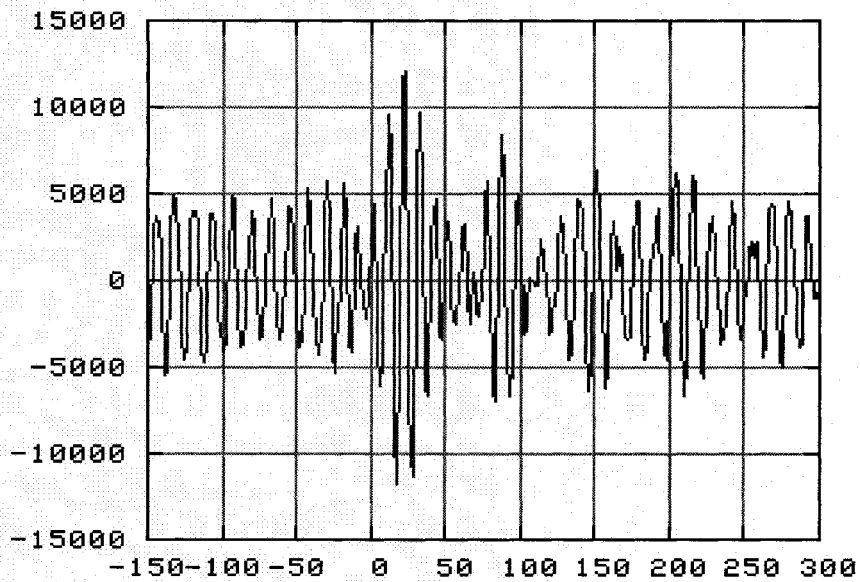


**Figure 4.11: Loran-C signal recorded in Denmark.**

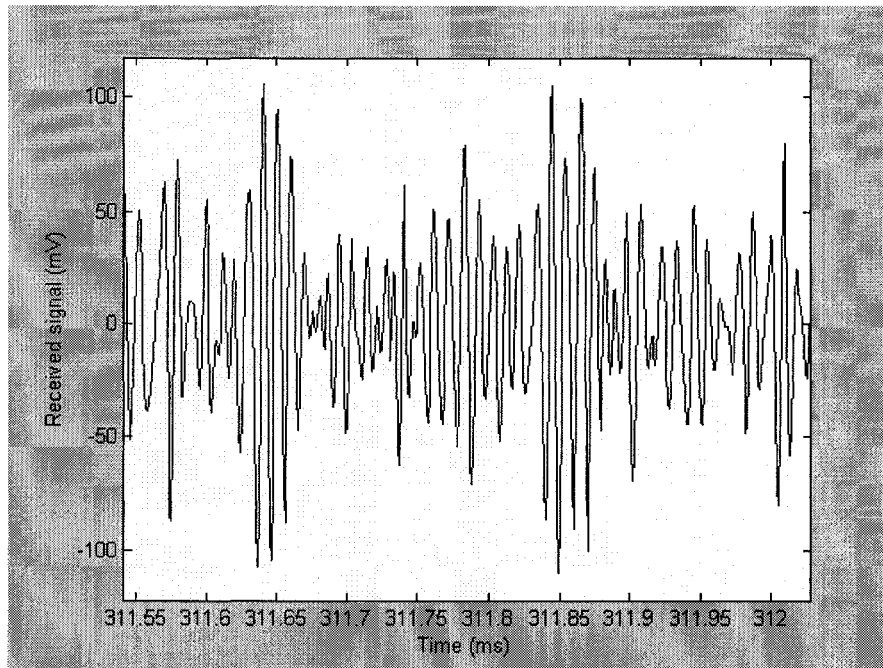


**Figure 4.12: Noise signal recorded at the CN Tower.**

In order to conclude the work of this thesis we need to discuss some more aspects of the comparison between simulated Loran-C signals as calculated at the location of the CN Tower and the actual captured noise waveforms and explain any inconsistencies.

As we have seen, the simulated Loran-C signal is almost always present, but there are considerable time frames where we do not have any signal. The simulation of the E-field at the location of the Tower is a very tedious procedure and we could only consider nine stations. However, Loran-C has a very long transmitting range and other stations from North America (and even Russia) can very well be received by the tower. Those signals will not be very powerful but will certainly affect the received signal. Furthermore, some Loran-C experimental stations exist which further complicate the situation. The Loran-C experimental station closest to the CN Tower is located at Wildwood, New Jersey and

transmits Loran-C signals using various radiating powers. Loran-C receivers are designed to eliminate these signals as they operate at different GRI's. The CN Tower obviously has no ability to separate the signals and receives the summation of all of them.

Although the simulated Loran-C signal resembles a lot the received noise signal, there is an apparent distortion of the received signal. Loran-C uses a phase coding system to assist the receivers in identifying a particular chain. Each pulse within a train of pulses is sent with a phase shift ( $0$  or  $\pi$ ) according to a unique code for each chain. This phase shift will result in distortion of the signal received by the Tower. Distortion in the form of frequency modulation will also occur because of the arbitrary phases when different signals are added. As it has been mentioned in Section 4.1 that lightning causes interference to Loran-C signals, but we can imagine that the CN Tower may also pick up other low-frequency signals that further distort the signal.

The detailed investigations performed in this thesis has proven that the low-frequency noise corrupting the CN Tower lightning current derivative waveforms is the Loran-C signal. This is a major contribution not only for the CN Tower lightning project but also for any other research related to measurement of lightning at tall structures. Researchers and experimentalists should be aware of the existence of the Loran-C signals and take necessary precautions to avoid its interference effect. The most effective precaution according to our experience is hardware protection using highly shielded measurement systems.

The work done in this thesis is also expected to help in the successful removal of the low-frequency noise from the recorded current derivative waveforms. Now that much more is known about the nature of the noise and its source, researchers may be able to utilize the pre-trigger portion of the recorded lightning waveforms (containing only noise) to denoise the CN Tower current derivative signals, possibly in the time domain.

# Chapter 5

## Conclusions and recommendations

The low-frequency noise corrupting the lightning current derivative signals measured at the CN Tower has been a source of trouble for the proper utilization of CN Tower lightning current data for the past 13 years. The existence of this noise makes the extraction of the current waveform parameters (peak, maximum steepness, risetime and pulse width at half peak value) very difficult. The derivation of comprehensive statistics of lightning current waveform parameters is essential for the establishment of more sophisticated protective measures against lightning hazards. Although a new current derivative measurement system that effectively shields the recorded waveforms from the low-frequency noise was installed in 1997, the amount of valid data captured by the new coil is too limited for statistical analysis. In order to utilize the large amounts of data captured by the old coil, the characterization of the low-frequency noise is of great importance.

During the past many years, while the emphasis has been placed on the removal of the low-frequency noise, no serious attempt was made to characterize this low-frequency noise and determine its source. In this thesis, the low frequency noise has been successfully characterized and its source has been identified.

The detailed investigations followed in this thesis has proven that the low-frequency noise corrupting the CN Tower lightning current derivative signals is the Loran-C signal. Loran-C is a radionavigation system using the frequency band of 90-110 kHz. Initially a major question of whether the interfering noise is a measurement related noise or an external signal was answered through special measurements performed at the location of the new coil. The results of these measurements proved that the low-frequency noise is caused by an external signal. Then a thorough analysis was performed in order to determine its source. The source was identified as the Loran-C signal.

This is a major contribution not only for the CN Tower lightning project but also for any other research related to measurement of lightning currents at tall structures. Researchers and experimentalists should be aware of the existence of the Loran-C signal and take the necessary precautions to avoid its interference effect. The most effective precaution according to our experience is hardware protection using highly shielded measurement systems.

The work done in this thesis is also expected to help in the successful removal of the low-frequency noise from the recorded current derivative waveforms. The information obtained about the nature of the noise and its source is expected to help in utilizing the pre-trigger portion of the recorded lightning current derivative waveforms (containing only noise) to denoise the CN Tower current derivative signals, possibly in the time domain.

# References

- [1] A. Rakov and M.A. Uman, *Lightning: Physics and Effects*, Cambridge University Press, 2003.
- [2] A.M. Hussein, W. Janischewskyj, J.S. Chang, V. Shostak, W.A. Chisholm, P. Dzurevych, and Z.I. Kawasaki, "Simultaneous measurement of lightning parameters for strokes to the Toronto CN Tower," *Journal of Geophysical Research-Atmosphere*, vol 100, no. 5, pp. 8853-8861, May 1995.
- [3] W. Janischewskyj, A.M. Hussein, V. Shostak, I. Rusan, J.X. Liand J.S. Chang, "Statistics of lightning strikes to the Toronto CN Tower (1978-1995)," *IEEE Trans. Power Delivery*, vol. 12, no .3, pp 1210-1221, July 1997.
- [4] F. Rachidi, W Janischewskyj, A.M. Hussein, C.A Nucci, S. Guerrieri, B Kordi and J.S Chang, "Current and electromagnetic field associated with lightning-return strokes to tall towers," *IEEE Trans. On EMC*, vol 43, no .3 pp. 356-367, Aug.2001.
- [5] C.A. Nucci, G. Diendorfer, M.A. Uman, F. Rachidi and C. Mazzeti, "Lightning return-stroke models with channel-base specified current: A review and comparison," *Journal of Geophysical Research*, vol. 95m, pp. 20395-20408, Nov. 1990.
- [6] A.M. Hussein, W Janischewskyj, M. Milewski, V. Shostak, J.S. Chang and W.A. Chisholm, "Return stroke current waveform parameters of lightning to the CN Tower (1992-2001)," *Proceedings of the 26<sup>th</sup> International Conference on Lightning Protection*, pp. 161-166, Cracow, Poland, Sept. 2-6, 2002.

- [7] A.M. Hussein, W Janischewskyj, M. Milewski, V. Shostak, F. Rachidi and J.S. Chang, "Comparison of current characteristics of lightning strokes measured at the CN Tower and at other elevated objects," IEEE Symposium on Electromagnetic Compatibility, Boston, MA, Aug. 18-22, 2003, Paper #149 (pp. 1-6).
- [8] A.M. Hussein, W Janischewskyj, M. Milewski, A. Siddiqi, V. Shostak and J.S. Chang, "Parameters of radiated fields from CN Tower and non-CN Tower lightning strikes," IEEE Bologna Power Tech Conference, Bologna, Italy, June 23-26, 2003, Paper #460 (pp. 1-8).
- [9] M. Milewski, "Statistical analysis of CN Tower lightning current parameters (1992-2001)," MAsc. Thesis, University of Western Ontario, London, ON, January 2003.
- [10] W. Janischewskyj, A.M. Hussein and V. Shostak, "Propagation of lightning current within the CN Tower," CIGRE SC 33.97, Toronto, Ontario, Canada, Sept. 2-3, 1997.
- [11] W. Janischewskyj, A.M. Hussein and J.S. Chang, "Characteristics of CN Tower multistroke flashes," 10<sup>th</sup> International Symposium on High Voltage Engineering, Montreal, Quebec, Aug. 1997.
- [12] M.J. Islam, "De-Noising The CN Tower Lightning Current Signal Using Short Term Fourier Transform-Based Spectral Subtraction," MAsc. Thesis, Ryerson University, Toronto, ON, August 2003.
- [13] O. Nedjah and A.M. Hussein, R. Soludeh and W. Janischewskyj, "Wavelet noise removal from CN Tower lightning current waveforms," International Signal Processing Conference, Paper #505 (pp. 1-6), Dallas, Texas, Mar. 31-Apr. 3, 2003.
- [14] A. Obaid, "Improving the SNR of lightning records captured at the CN Tower using linear filtering techniques," B.A.Sc. Thesis, University of Toronto, Toronto, Ontario, Apr. 1993.

- [15] A.K. Ziarani, "Extraction of Non-Stationary Sinusoids," PhD Thesis, Electrical and Computer Engineering, University of Toronto, Toronto, ON, December, 1993.
- [16] M.J. Islam and A.M. Hussein, "A novel technique for de-noising the CN Tower lightning current signal by modifying its Fast Fourier Transform," International Signal Processing Conference (ISPC), 2003, Paper #287, pp 1-5, Dallas, USA, March 31-April 3, 2003.
- [17] S. Krishnan, Notes from the Ryerson University graduate course: "Adaptive Signal Processing," Toronto, Ontario, 2002.
- [18] Dimitris G. Manolakis, Vinay K. Ingle and Stephen M. Kogon, Statistical and Adaptive Signal Processing, Mc Graw Hill, 2000.
- [19] J. Astola and P. Kuosmanen, Fundamentals of nonlinear digital filtering, CRC Press, 1997.
- [20] L. Yin, and R. Yang, "Weighted Median Filters: A Tutorial," IEEE Trans. on Circuits and Systems-II: Analog and Digital Signal Processing, Vol. 43, No 3. March 1996.
- [21] E. Ifeachor and B.W. Jerwis, Digital Signal Processing: A practical approach, Addison-Wesley Pub Co, June 1993.
- [22] USCG, Loran-C User Handbook, 1990.
- [23] USCG, Specification of the transmitted Loran-C signal, COMDTINST M16562.4A, 1994.
- [24] J.D. Last, R.G. Farnworth and M.D. Searle, "Effect of skywave interference on the coverage of Loran-C," IEE Proceedings-F, Vol. 139, No. 4, August 1992.

[25] L.P. Remmerswaal and D. van Willigen, "Some aspects of interference on Loran-C," IEE Proceedings, Vol. 136, No. 3, June 1989.

[26] M.N.O. Sadiku, Elements of Electromagnetics, 3<sup>rd</sup> ed., Oxford University Press, New York-Oxford, 2001, chapter 13.

[27] ITU Recommendation, ITU-R P.368-7, "Groundwave propagation curves for frequencies between 10 kHz and 30 MHz," 1992

[28] [www.geod.nrcan.gc.ca/index\\_e/online\\_apps\\_e/appINDIR\\_e/terminverse\\_e.html](http://www.geod.nrcan.gc.ca/index_e/online_apps_e/appINDIR_e/terminverse_e.html)